ELSEVIER

Contents lists available at ScienceDirect

Acta Materialia

journal homepage: www.elsevier.com/locate/actamat



Full length article

Grain boundary slip – twin transmission in titanium

Behnam Ahmadikia ^{a,*}, Leyun Wang ^b, M. Arul Kumar ^c, Irene J. Beyerlein ^{a,d}

- ^a Department of Mechanical Engineering, University of California at Santa Barbara, Santa Barbara, CA 93106, USA
- ^b School of Materials Science and Engineering, Shanghai Jiao Tong University, China
- ^c Materials Science and Technology Division. Los Alamos National Laboratory. Los Alamos. NM 87545. USA
- ^d Materials Department, University of California at Santa Barbara, Santa Barbara, CA 93106, USA

ARTICLE INFO

Keywords: Commercially pure titanium Strain localization Crystal plasticity Twinning Slip bands Transmission

ABSTRACT

Using a combination of mechanical testing, scanning electron microscopy, and a unified crystal plasticity framework for discrete intragranular shear localization, we investigate intense, localized slip bands on prismatic planes and $\{10\overline{1}2\}$ $\langle\overline{1}011\rangle$ tensile twins, and their transmission across the grain boundaries (GBs) in commercially pure titanium. The analyses show that the orientation and curvature of the GB influence the local stress fields at the GBs, and consequently, the slip/twin transmission across the boundary. In addition to host grain properties, neighboring grain properties, such as active slip systems and instances of heterogeneity like slip bands and twins, heavily affect the deformation mechanisms in each grain. Finally, the applicability of geometric factors to predict the transmission in the experimentally observed co-located pairs is discussed. The local stress field calculated by the discrete slip and twin band model is shown to be capable of determining whether a transmission has occurred in an observed co-located pair, and also the direction of the transmission.

1. Introduction

Commercially pure titanium (CP-Ti) and its alloys have been widely used in industry due to their superior mechanical properties, such as high specific strength, excellent corrosion resistance, and biocompatibility [1–5]. However, their plastic behavior can be highly anisotropic and strongly dependent on temperature and strain rate [6-9]. The complexity is due in part to the activation of two distinct deformation mechanisms-slip and twinning. Both heterogeneously shear the grain on crystallographic planes [10-14] and can grow in intensity in the form of bands that extend partly or fully across the grain [8,15-18]. Localized slip bands (SBs) and twin bands play a significant role in the deformation of Ti since they accommodate a large share of the parent grain's deformation while only occupying a small fraction of the grain's volume. These localized bands generate intense stress fields in the regions where the band terminates, whether inside the grain or at the grain boundary (GB). The latter is the more frequently observed case and, importantly, the situation that permits them to affect deformation mechanisms in the neighboring grains. They can, for instance, act as a potential site for strain localization and void nucleation [19,20]. They have also been seen to "transmit" and propagate across the GBs, potentially leading to long twin or SB chains that percolate across the

grain structure [21-24]. To what extent localized SBs or twins can alter deformation mechanisms in neighboring grains and the variables determining the propensity of such transmissions have long been key questions of interest.

Over the last few decades, several experimental studies have employed imaging techniques to study twin and SB transmissions across GBs in polycrystalline Ti alloys, as well as other structural hexagonal close-packed (HCP) metals [15,16,25–31]. In the post-mortem surface techniques, microscopic signatures of the slip or twin transmission are "co-located" pairs, a term that refers to a pair of slip and/or twin bands, each embedded in a different grain, intersecting the shared GB at nearly the same location. Slip-band pairs, twin pairs, or mixed slip/twin pairs have all been reported to occur frequently, suggesting that they are a non-negligible contributor to plastic deformation [8,15,27–29,32]. Significantly, another study demonstrated that such co-located pairs were not a surface effect and occurred subsurface as well [16].

To understand the conditions for transmissions, a geometric factor, $m^{'}=(n_i\ .\ n_o)\cdot(b_i\ .\ b_o)$ is often used. The $m^{'}$ gauges the alignment of the planes, with normal vectors of n, and the shear directions, denoted by b, of the incoming (i) and outgoing (o) slip or twin systems in question [33]. It helps to identify the most likely SB system or twin variant that would form in the neighboring grain, should a transmission event occur.

E-mail address: behnam_ahmadikia@ucsb.edu (B. Ahmadikia).

^{*} Corresponding author.

Table 1 Composition of grade 1 CP-Ti. All measurements are in wt.%.

Element	0	Fe	Al	Cu	С	Ni	Cr	S	N	Ti
wt.%	0.169	0.049	0.017	0.017	0.015	0.013	0.011	0.011	0.004	bal.

It tends to suggest that transmissions are more favored the lower GB misorientation, a tendency that indeed is generally observed [34,35].

While easy to use, several studies have demonstrated that additional variables, not accounted for in m', must also govern slip and twin transmissions [28-30,36-40]. Using post-mortem back-scattered diffraction (EBSD), Wang et al. reported a correlation in location across the GB between prismatic SBs in geometrically soft grains and $\{10\overline{1}2\}\langle\overline{1}011\rangle$ tensile twins in geometrically hard neighboring grains [15]. They found that m' of the observed co-located slip-twin pairs do not always correspond to the highest m' value possible between the pair of grains. High-resolution EBSD and differential aperture X-ray Laue micro-diffraction analyses of localized SBs in CP-Ti further showed that a high value of m is not necessarily associated with SB transmission across the GB [25,26]. A study on HCP Mg-Y alloy also found that m' cannot explain some of the observed slip-to-twin transmissions across GBs [36]. A machine learning model, using only grain orientations, failed to predict twins resulting from twin-twin transmissions at both low-angle and high-angle GBs [40]. Finally, a recent study in CP-Ti revealed that the morphology of the GB influences slip transmission across the GB [30]. They used electron channeling contrast imaging (ECCI) coupled with controlled surface removal to investigate the interaction of SBs with the GB as a function of depth. The slip system onto which incoming SBs transmit across the same GB was found to vary at different depths due to the fact that the orientation of the GB with respect to the incoming SBs varies between the surface and subsurface levels.

In addition to microstructural variables, it has been suggested that local stress fields produced by the bands themselves promote transmission and can determine the twin variant or SB system that will subsequently form on the other side of the GB [16]. Slip or twin bands can generate intense stress fields in the neighboring grains at the band/grain boundary junction. The intensity and character of these fields can differ from the grain average stresses in the neighboring grain and potentially promote slip or twinning activity that would not otherwise occur. One way of resolving such stress fields within a group of HCP grains is to utilize spatially resolved micromechanical techniques that can model localized intragranular bands and their interactions with GBs. In recent years, a few theoretical approaches [41,42], as well as several numerical methods, ranging from finite element (FE) method [43–51] to phase-field models [52–55] to fast Fourier transform (FFT) calculations [35,56-62], have been developed to model discrete SBs or twin lamellae within a grain and the stress fields ahead of them. Most of them were based on crystal plasticity, which enables deformation via anisotropic elasticity and multiple slip modes of the HCP crystal. One study implemented discrete SB modeling in an FFT-based elasto-viscoplastic formulation to study the shear localization for a range of HCP metals, including CP-Ti [56]. Neighboring grain orientations were found to influence SB intensification, and in turn, the type of band (prismatic or basal) in one grain was found to substantially alter the active deformation modes in the neighboring grain within the vicinity of the GB. A few more studies performed explicit twinning simulations using crystal plasticity-based models to calculate stress fields ahead of twin/GB junctions relevant for understanding twin-twin transmissions [35,63, 64]. Most of these studies only address the formation of a slip or twin band, and in cases where the localized stress fields ahead of the band is studied, only the transmission between two SBs or between two twin bands were considered, leaving the transmission between a SB and a twin uninvestigated.

The present work examines the grain neighborhood-induced twin or

slip localizations in CP-Ti. Combining scanning electron microscopy (SEM) analysis and crystal plasticity FFT modeling, we aim to elucidate the key factors that govern the transmission of slip and twin bands across the GBs. The model employed here features both discrete intragranular SBs and twin lamellae in the same microstructure. Different deformation modes are characterized in CP-Ti samples subjected to four-point bending. Prevalent at several GBs are co-located pairs of prismatic SBs and $\{10\overline{1}2\}\ \langle \overline{1}011\rangle$ tensile twins connected across a GB. Many of these pairs are analyzed via SEM and represented directly in simulations, with retention of the actual GB morphology and the orientation of the twin/ slip band with respect to the GB and loading direction. In many cases, the geometric m' fails to rationalize them. We demonstrate how calculation of the local stress fields helps to explain the occurrence of slip vs. twin transmission or the lack of transmission, and the selection of outgoing slip system or twin variant. It also helps to identify the transmission pathway (i.e., slip \rightarrow twin or twin \rightarrow slip) for the experimentally observed co-located pairs. The results indicate that the deformation mechanisms in one grain can be strongly affected by those of its neighboring grains, and the transmitted mechanism does not necessarily match the slip/twin system active in those grains.

2. Experimental methods and material characteristics

To characterize the transmission of slip/twin bands across the GBs, a rolled and recrystallized grade 1 commercially pure titanium (CP-Ti) is selected and subjected to four-point bending. The initial and deformed microstructures were characterized using a JEOL 6500 SEM equipped with an orientation imaging microscopy (OIM) system (EDAX/ TSL, Draper, UT). The mechanical test and a few initial microstructural characterizations have been previously carried out and are described in [8,15]. Some of the microscopy data from that experiment are newly presented here. So that the paper is self-contained, a brief description of the testing and characterization methods is given here.

Table 1 provides the chemical composition of the selected material system. To prepare the material for the four-point bend test, a 25mm-long specimen with a rectangular cross-section of 3mm \times 2.5 mm was cut such that the bulk of the grains have their c-axes oriented $\sim 45^{\circ}$ from the tensile axis of the bending sample. The specimen surface (25 mm × 3 mm) was mechanically polished before deformation. For high quality, visibly scratch-free surface, a final polishing was performed with a colloidal silica suspension. EBSD analysis in an area of $5 \text{ mm} \times 3 \text{mm}$ in the center of the surface of the specimen prior to deformation was performed. The initial material had a typical basal texture with an intensity of ≈ 6 multiples of random distribution with a grain size of 80µm. The specimen was then subjected to a four-point bending test so that the central region of its surface experienced uniform tensile stress along the sample longitudinal direction [65]. A surface tensile strain of ~2% was applied to ensure enough of the grains in the sample were plastically deformed. post-mortem EBSD investigations were conducted in the same 5mm $\, imes\,$ 3mm region located in the center of the surface, using the same imaging parameters. Intense SBs and twins on the surface were characterized via trace analysis and using the EBSD

3. Computational framework

3.1. Discrete slip/twin band crystal plasticity formulations

An infinitesimal-strain crystal plasticity (CP) model based on fast

Table 2 Softening coefficient D_0 , elastic constants [82], c/a ratio [83], and critical resolved shear stress (CRSS) values [81] for different deformation modes available for CP-Ti. Note that only slip modes are allowed to accommodate plastic deformation in the calculations.

Material	D_0	c/a		Elast	ic constants	(GPa)			CRSS values for	deformation modes (MPa)	
		ratio	C ₁₁	C ₁₂	C ₁₃	C ₃₃	C ₄₄	Prismatic $\langle a \rangle$	Basal $\langle a \rangle$	Pyramidal $I \langle c + a \rangle$	Tensile twin
CP-Ti	50	1.588	162.4	92.0	69.0	180.7	46.7	96	127	240	225

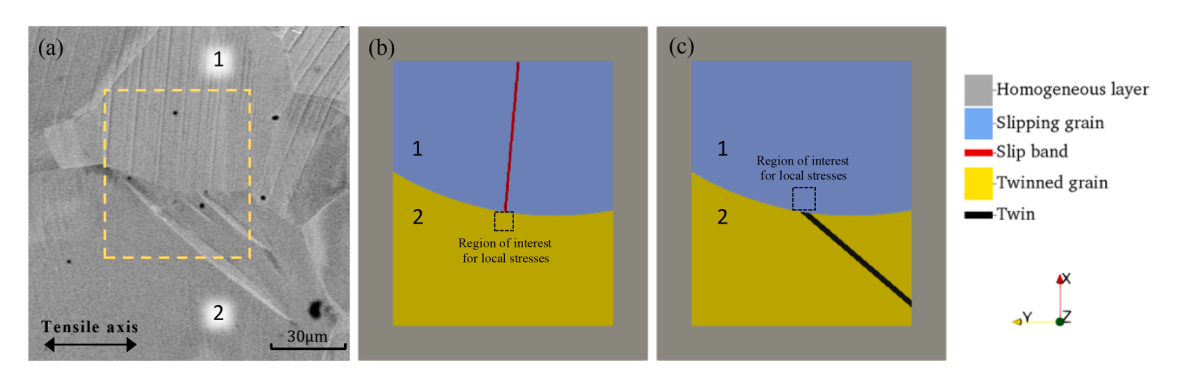


Fig. 1. (a) SEM image showing intense prismatic SBs in grain #1 and $\{10\overline{1}2\}$ twin lamellae in grain #2. Dashed lines indicate the border of the simulation cell. (b) Schematic of the bicrystal unit cell subjected to the SB constitutive law to examine potential slip-twin transmission. A 2-voxel-thick ($w_s = 2$) SB is embedded in the top grain, impinged at the curved GB. (c) The bicrystal unit cell simulated with the twinning constitutive law to study potential twin-slip transmission. A 6-voxel-thick ($w_t = 6$) black domain in the bottom grain shows the preselected area for twinning. In both (b) and (c), the dashed black box shows the region of interest in which the local stresses at the tip of the slip/twin band are assessed. The SEM image corresponds to pair P4 of Table 3.

Fourier transform (FFT) is employed in the present study. This full-field computational scheme, originally developed by Lebensohn et al. [66], has been advanced to capture intergranular heterogeneity in the form of intense SBs [56–58] and deformation twinning [59,67,68] in separate studies. Here we combine these two techniques to simulate heterogeneous elasto-viscoplastic deformation in CP-Ti crystals in which both intense SBs and deformation twins exist. For this reason, both formulations are briefly reviewed.

In the CP-FFT approach, a compatible strain field is adjusted to an equilibrated stress field by minimizing the average local work at each discretization point in several iterations [66]. The stress-strain relationship of an elasto-viscoplastic material with shear transformation is given by,

$$\sigma(\mathbf{x}) = \mathbf{C}(\mathbf{x}) : \mathbf{\varepsilon}^{\mathbf{e}}(\mathbf{x}) = \mathbf{C}(\mathbf{x}) : (\mathbf{\varepsilon}(\mathbf{x}) - \mathbf{\varepsilon}^{\mathbf{p}}(\mathbf{x}) - \mathbf{\varepsilon}^{\mathrm{tr}}(\mathbf{x}))$$
 (1)

where $\sigma(x)$ is the Cauchy stress tensor, C(x) is the tensor of elastic moduli, $\epsilon(x)$, $\epsilon^\epsilon(x)$, $\epsilon^\rho(x)$, and $\epsilon^{tr}(x)$ are, respectively, the total, elastic, plastic, and transformation strain tensors, calculated at any material point x. Twinning is modeled as a strain transformation process and the associated transformation strain $\epsilon^{tr}(x)$ applies only to points within the twin domain [59,67,68]. This shear transformation tensor is null in all points outside of the twin domains, including those associated with SBs. Using a semi-implicit time discretization scheme, the stress state in the material point x at time $t + \Delta t$ can be written as,

$$\begin{split} \boldsymbol{\sigma}^{r+\Delta t}(\boldsymbol{x}) &= \boldsymbol{C}(\boldsymbol{x}) \\ &: (\boldsymbol{\epsilon}^{r+\Delta t}\ (\boldsymbol{x}) - \boldsymbol{\epsilon}^{p,t}(\boldsymbol{x}) - \dot{\boldsymbol{\epsilon}}^{p,r+\Delta t}(\boldsymbol{x},\boldsymbol{\sigma}^{r+\Delta t})\ \Delta t - \boldsymbol{\epsilon}^{tr,t}(\boldsymbol{x}) - \Delta \boldsymbol{\epsilon}^{tr,r+\Delta t}(\boldsymbol{x})) \end{split} \tag{2}$$

The viscoplastic strain-rate tensor at material point \mathbf{x} , $\dot{\epsilon}^p(\mathbf{x})$, is constitutively calculated from the stress tensor through a sum over the N available slip systems, as follows:

$$\dot{\varepsilon}^{p}(\mathbf{x}) = \sum_{s=1}^{N} \mathbf{m}^{s}(\mathbf{x}) \ \dot{\gamma}^{s}(\mathbf{x}) = \dot{\gamma}_{0} \sum_{s=1}^{N} \mathbf{m}^{s}(\mathbf{x}) \ \left(\frac{|\mathbf{m}^{s}(\mathbf{x}) : \mathbf{\sigma}(\mathbf{x})|}{\tau_{c}^{s}(\mathbf{x})}\right)^{n} \ \text{sgn} \ (\mathbf{m}^{s}(\mathbf{x}) \\
: \mathbf{\sigma}(\mathbf{x})) \tag{3}$$

The change in transformation strain during the twinning process is

specified as,

$$\Delta \epsilon^{tr}(x) = \ m^{tw}(x) \ \Delta \gamma^{tw}(x), \ \Delta \gamma^{tw}(x) = \frac{S^{tw}}{N^{tw}..inc} \eqno(4)$$

In Eq. (3), $\dot{\gamma}^s(\mathbf{x})$, and $\tau_c^s(\mathbf{x})$ are, respectively, the shear rate and the critical resolved shear stress (CRSS), associated with slip system s at point \mathbf{x} . Furthermore, $\dot{\gamma}_0$ is a normalization factor and n is the stress exponent. $\mathbf{m}^s = 1/2 \ (\mathbf{b}^s \otimes \mathbf{n}^s + \mathbf{n}^s \otimes \mathbf{b}^s)$ and $\mathbf{m}^{tw} = 1/2 \ (\mathbf{b}^{tw} \otimes \mathbf{n}^{tw} + \mathbf{n}^{tw} \otimes \mathbf{b}^{tw})$ are, respectively, the Schmid tensors associated with the slip system s and the twinning system. Unit vectors $\mathbf{b}^s \ (\mathbf{b}^{tw})$ and $\mathbf{n}^s \ (\mathbf{n}^{tw})$ are aligned with the slip (twinning) shear direction, and slip (twin) plane normal. Finally, in Eq. (4), N^{tw_inc} is the number of increments by which the shear strain in the twin domain, $\Delta \gamma^{tw}$, reaches the characteristic twin shear, S^{tw} .

For material points corresponding to SBs, $\mathbf{x} \in SB$ domain, a different procedure is applied. Strain localization in polycrystals developed by recurring glide within intense SBs is associated with low or negative strain hardening in many experimental studies [69–78]. Moreover, extensive crystal plasticity modeling studies consider SBs as domains undergoing material softening, i.e., a decay in the slip resistance with strain [41–49,56–58,79]. In these models, softening only occurs for active slip systems in the band and at the rate at which it slips. To characterize such behavior, the critical resolved shear stress $(r_{\rm c}^{\rm s})$ for any slip system s decays linearly with the rate of plastic strain $(\dot{r}^{\rm s})$ on that system at each material point \mathbf{x} located within a preselected band, while the resistance to slip on all systems at all material points outside the band will be fixed throughout the simulation:

$$\tau_{c}^{s,t+\Delta t}(\mathbf{x}) = \begin{cases} \tau_{c}^{s,t}(\mathbf{x}) - D_{0} \ \tau_{c}^{s,t}(\mathbf{x}) \ |\dot{\gamma}^{s,t}(\mathbf{x})| \ \Delta t & \mathbf{x} \in SB \ domain \\ \tau_{c}^{s,t}(\mathbf{x}) = \tau_{c}^{s}(\mathbf{x})|_{\gamma^{s}(\mathbf{x})=0} & \mathbf{x} \notin SB \ domain \end{cases}$$
(5)

where the coefficient D_0 in Eq. (5) is a material constant to regulate the rate of softening. It is suggested to calibrate the model using experimental results to obtain an accurate measure for D_0 . However, in the present study, this constant is numerically determined so that the experimentally observed SBs fully develop within the prescribed applied strain. To avoid numerical instabilities, a lower limit of $\tau_c^s=2$ MPa is set for all slip systems.

Fig. 2. (a) SEM image reveals pair P3 with slip \leftrightarrow twin transmission across the GB in a CP-Ti sample subjected to 2% uniaxial strain along the y-axis. The box with dashed lines shows the frame from which computational models are built. Models constructed with (b) an actual or (c) a planar GB morphology for the pair of grains in (a). In both models (b-c), a 2-voxel-thick SB is embedded in grain #1.

3.2. Material parameters and model setup

Material parameters used in the calculations include the single-crystal elastic constants at room temperature, available slip systems, and their critical resolved shear stress (CRSS) values, the lattice constant (c/a ratio), and the coefficient D_0 in Eq. (5). These are presented for CP-Ti in Table 2. CP-Ti has an anisotropy index 1 of $A^L=0.075$, where the ideal case of perfect isotropy yields zero [80], showing more elastic anisotropy than many common HCP metals, like Mg ($A^L=0.012$) and Zr ($A^L=0.046$). We made available to the calculation the dominant slip systems reported in experimental studies [15,28,32,81]. These are prismatic $\langle a \rangle$, basal $\langle a \rangle$, and pyramidal $\{10\overline{1}1\}$ $\langle 11\overline{2}3 \rangle$ slip. Considering plastic deformation, the easiest slip mode in Ti is prismatic slip, followed by moderately harder basal slip, and then pyramidal $\langle c+a \rangle$ as the hardest mode [81]. For comparison, a reported CRSS value for $\{10\overline{1}2\}$ tensile twinning is also given in Table 2, although it is not used or needed in the calculations.

Crystalline microstructures are modeled here that mirror those observed experimentally, both previously published [8,15] and newly presented data, including material points associated with discrete twin lamellae and SBs. Fig. 1 shows an example comprising a grain with many prismatic SBs neighboring a grain with a few twin lamellae. The box with dashed lines in Fig. 1(a) shows the frame from which the bicrystals are created for the calculations. Fig. 1(b) and (c) show the microstructure models used for the corresponding SB and twin band, respectively. The decomposition of a co-located pair into uncoupled, independent simulations of SB and twin band allows the analysis of the local stress fields ahead of each band and helps to identify whether the pair developed via a directional "path-dependent transmission" or an independent "co-formation" event. The bicrystals in Fig. 1(b) and (c) are discretized into 250×300 voxels in the y- and x-direction, respectively. A SB domain is preselected within the banded grain to mirror the SEM image. The actual imaged domain corresponds to the intersection of the dominant glide plane with the viewing x-y plane. For all SBs modeled here, two voxels span the SB thickness. This thickness is sufficiently fine to enable a uniform shear through the thickness of the band [56]. To model the discrete twin bands in all calculations, a six-voxel-thick twin domain is embedded in its parent crystal, as shown in Fig. 1(c). The out-of-plane thickness of the bicrystals spans three voxels in all calculations. It can be shown that greater (by two orders of magnitude) simulation cell thicknesses do not change the calculated micromechanical fields [56]. All simulation cells are surrounded by a 40-voxel-thick layer in both in-plane directions with properties of a randomly oriented CP-Ti polycrystal. The thickness of this layer is sufficiently

large to render spatially resolved micromechanical fields insensitive to the image forces due to the considered periodic boundary condition.

The CPFFT simulation cells are subjected to uniaxial tension along the y-direction, up to 2% strain, consistent with the actual experimental condition. Normal stress components in the other two directions are enforced to be zero. Modeling slip banding and twinning are performed sequentially. In the SB simulations, the constitutive law stated in Eq. (5) is applied to the material points inside/outside the band domain, and no shear transformation or reorientation is involved. Macroscopic strain is set to evolve in increments of 0.01% per time step and the time steps are specified to be small enough to ensure convergence. When modeling the twin lamella, the same level of uniaxial strain is first applied to the simulation cell without the twin. Subsequently, the lattice of the twin domain is reoriented following the twin/matrix orientation relationship, and the characteristic twin shear is built incrementally and homogeneously over $N^{tw_inc} = 2000$ increments, according to Eq. (4). Considering that twinning occurs on much faster time scales than slip, we model slip as a rate sensitive process, in which plasticity develops in time with strain, and twinning as a relatively instantaneous process. We insert the twin at a fixed time step, rather than modeling its growth over time. Thus, the incremental implementation of the twin shear is only to ensure numerical convergence and occurs at a fixed macroscopic strain level, signifying the instantaneity of twinning relative to slip. Although not an inherent limitation of the present formulation, hardening in the CRSS values for basal and prismatic slip are not included for the sake of simplicity in the calculations. The competition between these two modes is not expected to change significantly within the few percent of applied

In all calculations, as in Fig. 1, we consider the actual GB plane morphology and crystal orientations. The shear tractions calculated along the boundary because of local GB curvature or inclination with respect to macroscopic load are expected to contribute to the local stresses and potentially play a role in the propensity for band transmission. To elucidate the GB morphology effect, we repeat some calculations for a simplified geometry consisting of two equal-sized grains sharing a planar GB, as seen in Fig. 2(c). For both actual and planar GBs, two sets of simulations are conducted, one with and the other without the slip/twin band modeled in their parent grain. The calculated local stresses ahead of the band, at the GB junction within the neighboring grain, particularly over a region that is several times the thickness of the band, as indicated in Fig. 1(b) and (c) with dashed black boxes are compared.

To identify the deformation mode and system onto which a transmission from an experimentally observed slip/twin system is more likely to happen, when explicitly modeling either a discrete SB or twin, the system of the modeled band or twin corresponds to the experimentally observed system. However, in any material point outside of the band domain, all slip systems are available for activation. Further, we consider all 18 slip systems and six variants of $\{10\overline{1}2\}$ tensile twinning, when identifying candidate slip/twin system in the neighboring grain

The anisotropic index is defined as: $A^L = \sqrt{\left[\ln\left(\frac{\nu^V}{k^R}\right)\right]^2 + 5\left[\ln\left(\frac{\mu^V}{\mu^R}\right)\right]^2}$, where $9\kappa^V = C_{11} + C_{22} + C_{33} + 2C_{12} + 2C_{13} + 2C_{23}, 15\mu^V = C_{11} + C_{22} + C_{33} - C_{12} - C_{13} - C_{23} + 3C_{44} + 3C_{55} + 3C_{66}, 1/\kappa^R = S_{11} + S_{22} + S_{33} + 2S_{12} + 2S_{13} + 2S_{23}, 15/\mu^R = 4 \left(S_{11} + S_{22} + S_{33} - S_{12} - S_{13} - S_{23} + 3S_{44} + 3S_{55} + 3S_{66}\right).$

Table 3 Orientation of the SB and twinned grains as well as the Schmid factors for the active systems and the geometric factor m' associated with the transmission. The deformation modes in all banded and twinned grains are prismatic slip (except for P6) and $\{10\overline{1}2\}$ tensile twin (T1), respectively. Refer to Table 4 for the variant's crystallographic details.

	Pair				Banded gr	rain					Гwinned / bar	ded grain		m′
		1	Euler angl	les	(Observed prismatic SB	_	E	uler angl	es	0	bserved T1 twinning /	SB	
		ϕ_1	Φ	ϕ_2	variant	Number of bands	m _s	ϕ_1	Φ	ϕ_2	variant	Number of bands	m _t or m _s	
$S \leftrightarrow T$	P1	77	65	288	2	27	0.48	159	87	196	1	5	0.43 ^b	0.93
	P2	68	74	291	2	17	0.44	313	93	131	6	6	0.23	0.89
	P3	93	123	356	3	21	0.47	20	105	348	2	3	0.38	0.88
	P4	91	80	281	2	23	0.50	26	83	339	2	3	0.39	0.79
$S \leftrightarrow S$	P5	59	78	295	2	5	0.37	67	84	292	1	5	0.27	0.27
	P6	82	80	257	3	31	0.49	147	63	76	$< c+a>^a$	8	0.41	0.03
s ⊣ 0	P7	95	75	68	3	10	0.49	12	82	143	-	0	-	-

^a Observed slip mode is $(\overline{1}011)$ $[2\overline{1}\overline{1}3]$ $\langle c+a \rangle$ pyramidal slip system.

for transmission. For instance, to determine the slip system onto which a twin transmits across the GB, we compare slip activity on all 18 systems at the twin tip and identify those with the highest activity as potential outgoing systems in a twin-to-slip transmission.

4. Results

4.1. Experimental results

Results from the current microstructural characterization of the deformed material along with detailed descriptions of some parts of the dataset that were previously published in [15] are presented here. Consistent with those descriptions in [15], trace analysis across the investigated surface area revealed that prismatic slip was prevalent in many grains in the part of the dataset newly presented here. The analysis also reveals the activation of substantial number of grains with T1: $\{10\overline{1}2\}$ tensile twins. Considering the twin volume fraction and the relatively low characteristic twin shear for T1 twins in CP-Ti, no more than approximately 4% of the total strain was accommodated via deformation twinning [15]. SEM image analysis shows a strong correlation between the twin lamellae and prismatic SBs in the grain neighbor in nearly one-third of the twinned grains.

Table 3 presents the crystallographic and geometric information obtained from the SEM/EBSD analysis for four pairs of twinned grains and "banded grains" (grains containing SBs) in which the SBs and twins (S \leftrightarrow T) were co-located, as well as two cases of co-located SBs on either side of the boundary (S \leftrightarrow S). For comparison, we include the same information for a grain containing lone SBs, blocked at the GB (S \dashv 0). Grain orientations are given by Euler angles in Bunge convention in a coordinate system with x= transverse, y= tensile axis, and z= sample normal. In some cases, several SB/twin co-located pairs were observed across the same boundary, and for these cases, the number of SBs or twins identified in each grain is included.

Before performing micromechanical calculations, a geometric analysis is performed for all the observed cases. Table 3 lists the Schmid factor for the observed slip (m_s) or twin (m_t) band system. The underlined Schmid factor entries, whether m_s or twinning m_t , indicate when the active SB or twinning variant is preferred, compared to all other slip or T1 twinning systems, by their parent orientation alone. Table 3 also

offers the geometric factor $m^{'}$ associated with the transmission. An underlined $m^{'}$ value means that, according to the $m^{'}$ criterion, the transmission is most favorable (i.e., has the highest $m^{'}$) among all prismatic slip – T1 twinning pairing in S \leftrightarrow T cases, or slip – slip pairing in S \leftrightarrow S cases. Crystallographic information about different variants of prismatic slip and tensile twinning is presented in Table 4.

One can obtain some quick insight from assessing these geometric factors. First, it is evident that the observed SB prismatic system in the banded grains in $S \leftrightarrow T$ cases has the highest Schmid factor between the three possible prismatic systems. The same conclusion, however, cannot be made for twinned grains as there are several grains in which the operating twin variant is not associated with the highest Schmid factor twin variant. When considering the combinations of prismatic SBs and twins, we find that the geometric factor m' becomes the better geometric predictor than the Schmid factor. A previous study [15] came to a similar conclusion, suggesting that grain with a twinning system that makes a high m' with respect to the incoming SBs is more likely to display slip-stimulated twinning. However, neither the Schmid factor nor m' indicates whether observed transmitted pairs were accomplished via co-formation or path-dependent transmission. Alternatively, analysis of the local stress field can indicate not only if the band transmits, but whether these pairs resulted from co-formation or path-dependent transmission and the sense of direction taken. To this end, in the calculations that follow, we decompose co-located pairs into two problems, each of which with just one slip or twin band, and analyze the stress field ahead of it in the neighboring grain.

4.2. Role of GB morphology on local stress field near the GB

Since local stress states are important for the analysis, we first investigate the effect of GB morphology, its curvature and orientation with respect to loading axis, on the local stress state, by comparing the GB shear traction developed for the actual morphology with that for a planar boundary. Fig. 2(a) shows a SEM image from pair P3 with prismatic SBs in grain #1 connected to twin lamellae in grain #2 across the GB. Bicrystals with the actual and planar GB morphologies are shown in Fig. 2(b) and (c), respectively. Both models are subjected to 2% applied strain along the y-direction, consistent with the experiments.

Table 4 Crystallographic information about different variants of prismatic slip and $\{10\overline{1}2\}$ tensile twinning.

		Prismatic slip				$\{10\overline{1}2\}$ tens	sile twinning		
Variant	1	2	3	1	2	3	4	5	6
Shear direction Plane normal	$\begin{array}{c} [2\overline{1}\overline{1}0] \\ (01\overline{1}0) \end{array}$	$\begin{array}{c} [\overline{1}2\overline{1}0] \\ (10\overline{1}0) \end{array}$	$\begin{array}{c} [11\overline{2}0] \\ (1\overline{1}00) \end{array}$	$[\overline{1}011]$ $(10\overline{1}2)$	$\begin{matrix} [0\overline{1}11] \\ (01\overline{1}2) \end{matrix}$	$\begin{array}{c} [1\overline{1}01] \\ (\overline{1}102) \end{array}$	$\begin{array}{c} [10\overline{1}1] \\ (\overline{1}012) \end{array}$	$\begin{matrix} [01\overline{1}1] \\ (0\overline{1}12) \end{matrix}$	$\begin{array}{c} [\overline{1}101] \\ (1\overline{1}02) \end{array}$

^b Both twin variants 1 and 5 have the highest Schmid factor in the twinned grain.

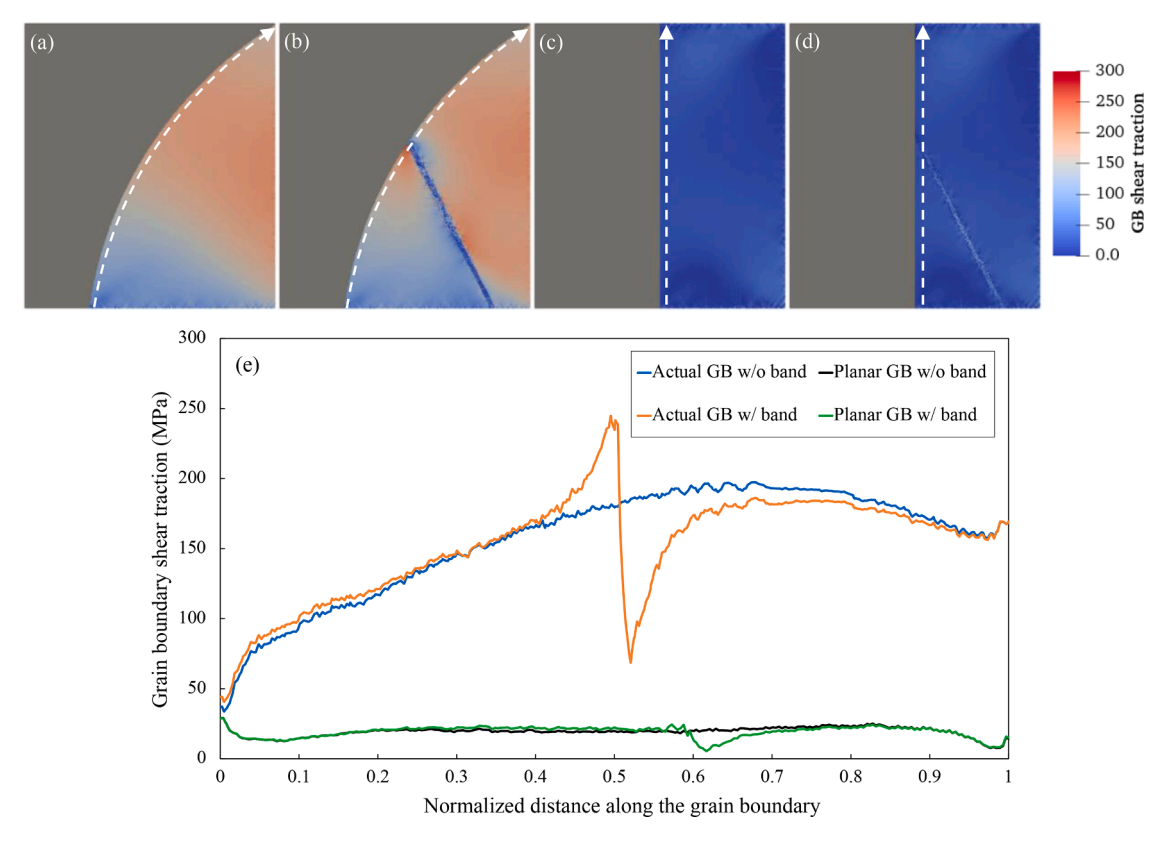


Fig. 3. Distribution of the GB shear traction in grain #1 at 2% macroscopic strain for the bicrystal with the actual GB morphology (a) without and (b) with an intense SB and (c-d) for the same bicrystal but with a planar GB (c) without and (d) with an intense SB, (e) Variation of the GB shear traction at 2% macroscopic strain calculated along the paths shown with white dashed lines in parts (a) through (d). The sudden drop in the two GB profiles with a SB corresponds to the location where the SB is crossed and is associated with the softening in the band. Distance along the GB is normalized by the length of the GB. Grain #2 is colored gray in parts (a-d) to help emphasize the fields in the grain #1 side of the GB. (For interpretation of the references to colour in this figure legend, the reader is referred to the web version of this article.)

Furthermore, to evaluate how SBs affect the GB shear traction, simulations are repeated with no active SB in grain #1.

Fig. 3(a–d) shows the distributions of the GB shear traction (τ_{GB}), on the grain #1 side of the boundary, for both actual and planar boundaries with and without a SB. The GB shear traction at each point near the boundary is calculated given the full stress tensor and the orientation of the GB at that point. Fig. 3 reveals a significant distinction between the GB shear tractions, signaling the imperative role GB orientation and curvature play. The cases containing a SB in Fig. 3(b, d) further demonstrate the discontinuity in the shear traction along the boundary at the band/GB junction caused by the SB. The shear traction varies significantly along the GB, a phenomenon that would have been missed if the actual morphology of the GB was not modeled. Finally, Fig. 3(e) compares the shear traction profiles between the actual GB morphology and the planar one. While in both cases the SB locally alters the stress fields, particularly at the SB/GB junction, the alteration is more substantial when the actual morphology of the GB is considered.

The results thus far quantitatively reveal a significant role of GB morphology on GB shear traction, a quantity that could contribute to slip transmission across the GB. This notion is consistent with prior studies [30,84]. An experimental investigation of the interaction of SBs with the GB as a function of depth in CP-Ti revealed that the slip system onto which incoming SBs transmit across the same GB can alter at different depths, only because the orientation of the GB with respect to the incoming SBs changes between two depths [30]. Furthermore, a molecular dynamics (MD) study [84] found that the resolved shear stress (RSS) contribution from the GB tractions either helps or hinders the

emission of dislocations, depending on their direction with respect to the RSS contribution from the applied loading. Accordingly, the actual morphology and orientation of GBs, as well as the orientation of SBs or twin domains, with respect to applied loading are preserved in all calculations that follow.

4.3. Simulation of potential slip-to-twin transmissions

In this section, we investigate a few cases to study the stress field developed at the tip of a SB inside the neighboring grain to identify whether they assist or prevent slip-to-twin transmission across the GB. Fig. 4(a) shows a SEM image of pair P2 in which parallel prismatic SBs in grain #1 are spatially correlated with $(1\overline{1}02)\ [\overline{1}101]$ twin lamellae in a relatively small neighboring grain #2 at 2% applied strain. Activated prismatic slip in grain #1 has a high Schmid factor of $m_s=0.44$, suggesting the possibility for the independent activation of SBs in this grain. In grain #2, on the other hand, the Schmid factor for the most favorable twin variant (V6), which is the same as the observed variant, is only $m_t=0.23$, signifying that this grain is not well oriented for twinning. Twin nucleation in small grains is particularly unlikely when the Schmid factor is low [85], further highlighting the role that SB localization in grain #1 could play in twin nucleation in grain #2, but not the other way around.

Due to the fact that the m' factor associated with the prismatic SBs in grain #1 and observed twin variant in grain #2 (m' = 0.89) is the highest among all other twin variants, it was previously conjectured that

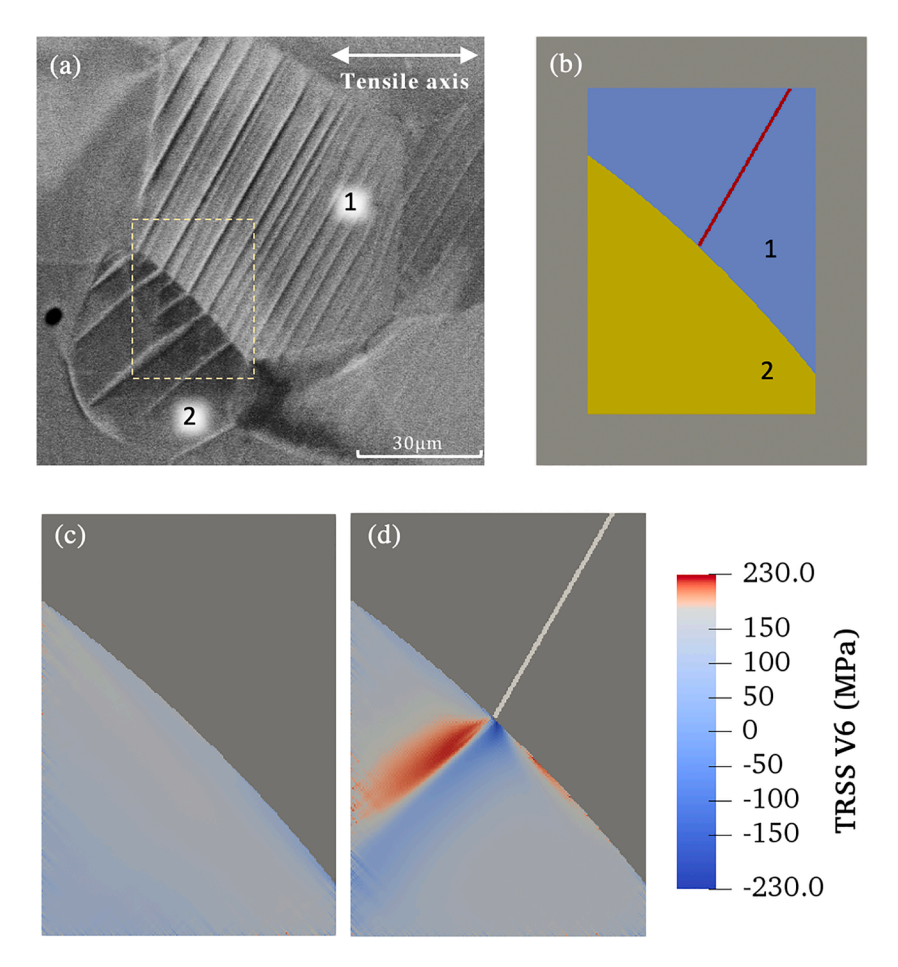


Fig. 4. (a) SEM image at 2% macroscopic strain for pair P2 revealing a possible transmission between intense prismatic SBs in grain #1 and $(1\overline{1}02)$ [$\overline{1}101$] tensile twin (variant 6) in grain #2 [$\overline{1}5$], (b) Bicrystal model for the pair P2 shown in (a), calculated field at 2% macroscopic strain of the twin plane resolved shear stress (TRSS) for the $(1\overline{1}02)$ [$\overline{1}101$] tensile twin variant (V6), (c) without and (d) with an intense SB in grain #1.

twin nucleation might have happened as a result of a local change in the stress fields at the GB caused by the prismatic slip activity localized in grain #1 [15]. However, the noteworthy questions are why easy prismatic slip with a slightly higher Schmid factor ($m_s=0.26$) did not form in grain #2 and why twins, with this variant, formed instead?

These questions can be addressed by investigating local stress fields at the SB tip for both mechanisms. Fig. 4(b) shows the bicrystal model used to study local stress fields at the tip of the prismatic SBs in grain #1. The other nearest and next nearest neighbors are not explicitly modeled, but rather the effect of the surrounding neighbors is represented by a

homogeneous medium. In the Appendix, we demonstrate for this pair that explicitly resolving more neighboring grains than in the current bicrystal model does not significantly affect the local stress fields in and around the slip band tip. Fig. 4(c) and (d) respectively, represent the distribution of the twin resolved shear stress (TRSS) for variant V6 $(1\overline{1}02)$ [$\overline{1}101$] seen in grain #2, for a simulation model with and without a SB in grain #1, both for 2% applied strain. In either case, we first find that the stress field in the two grains is heterogenous and unlike the farfield macroscopic stress, signifying the effect of the surrounding homogeneous medium on local stress distribution within these grains.

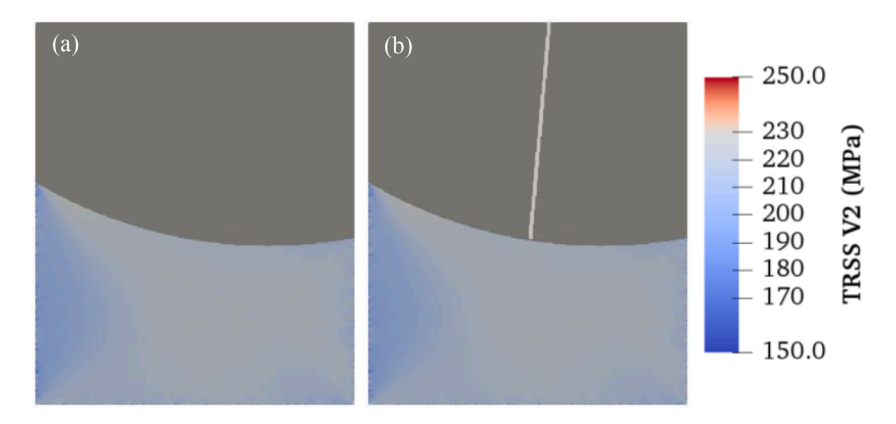


Fig. 5. Calculated twin plane resolved shear stress (TRSS) fields for the $(01\overline{1}2)$ $[0\overline{1}11]$ tensile twin variant (V2) at 2% macroscopic strain (a) without and (b) with an intense SB in grain #1. It is evident that the SB in this case does not affect the local driving stress for twinning at the tip.

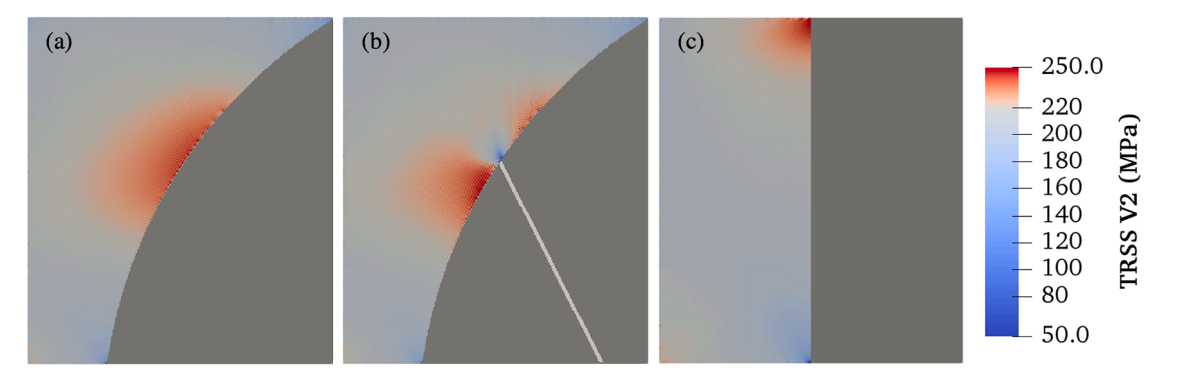


Fig. 6. Calculated distribution of the twin plane resolved shear stress (TRSS) in pair P3 for the $(01\overline{1}2)$ [$0\overline{1}11$] tensile twin variant (V2) at 2% macroscopic strain, with the actual GB morphology, and (a) without and (b) with a SB embedded in grain #1. Perhaps counterintuitively, the SB has decreased the TRSS in the vicinity of the SB, and thus reduces the possibility of slip to twin transmission across the boundary. (c) TRSS distribution in grain #2, for a planar GB without a SB, elucidating the effect of GB morphology on the local stress fields at the boundary.

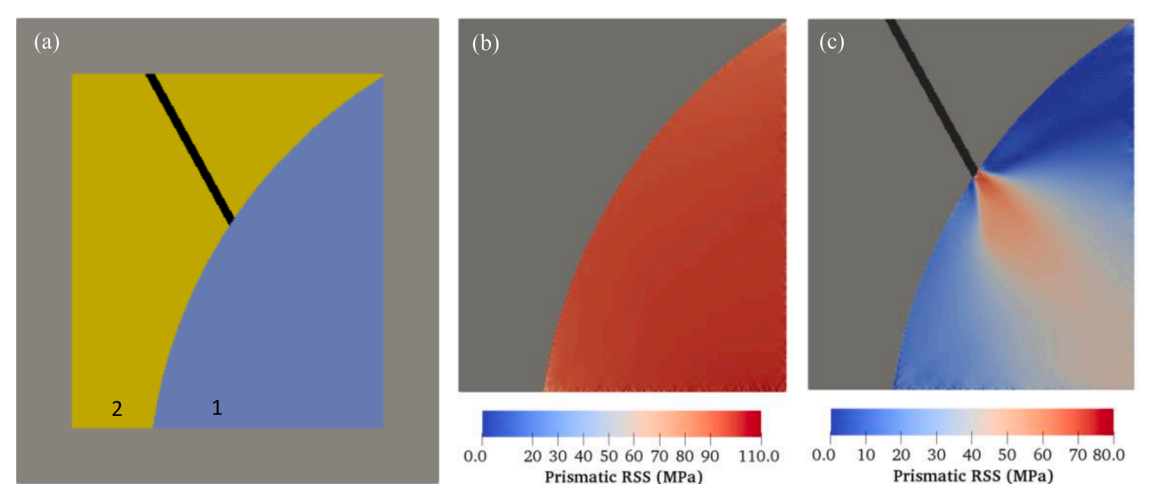


Fig. 7. (a) Bicrystal model for pair P3 shown in Fig. 2(a), with a twin lamella in black, (b-c) Calculated distribution of the resolved shear stress (RSS) for the prismatic slip system in grain #1, in which intense prismatic SBs are observed, at 2% strain, and (b) without the twin, and (c) with the twin.

Without a SB, the TRSS is uniformly distributed and low, suggesting twinning is not favored in grain #2 under the imposed 2% strain. With a SB, however, intense TRSS develops in grain #2 at the SB tip. The TRSS maps for the other five $\{10\overline{1}2\}$ twin variants find that variant V6 shown in Fig. 4 and seen experimentally, experiences the greatest intensity, which explains why V6 was selected. The difference in stress fields between the cases with and without a slip localization supports the idea that the enhanced stress field at the SB tip is responsible for the twins seen in grain #2.

Since slip competes with twinning, the driving forces for prismatic slip are also compared for these two cases to determine whether SB formation would have been favored over twinning. Evaluation of the prismatic slip system resolved shear stress fields in grain #2 indicates that the maximum RSS intensity at the SB tip is weakened by 18% with the SB than without. These calculations, therefore, suggest that the intense prismatic SBs in grain #1 initiated the twins in grain #2 despite the low Schmid factor of this variant, determining this co-located pair as a case of path-dependent transmission. In this case, the choice of deformation mechanisms, slip or twinning, of grain #2 was significantly influenced by the deformation behavior, particularly the localized SBs within neighboring grain #1.

To demonstrate a case in which SBs do not affect the stress fields in

the grain neighbor, the pair P4 shown in Fig. 1 is considered. In P4, grain #1 contains several parallel prismatic SBs, whereas $(01\overline{1}2)$ $[0\overline{1}11]$ twin (variant 2) is activated in grain #2. Grain #1 is perfectly oriented for prismatic slip with $m_s=0.5$ while the Schmid factor for the observed twin variant in grain #2 ($m_t=0.39$) as well as the transmission factor ($m^{'}=0.79$) are relatively high. Since the twin lamellae in grain #2 have terminated in the middle of the grain, we can argue that they initiated at the common GB of grains #1 and #2 and at locations where the SBs intersected it. However, whether SBs in grain #1 and twins in grain #2 were accomplished via co-formation or path-dependent transmission cannot be determined from the SEM image.

To gain insight into the sequence of events, contours of the TRSS for the operating twin variant (V2) after 2% applied strain are shown in Fig. 5(a) and (b), respectively, for a model without and with a SB embedded in grain #1. First, it is evident that the SB in grain #1 has no effect on the V2 TRSS field in grain #2. Second, analyzing the other variant TRSS fields finds that the SB would not serve as a driving force for any other twin variant. Last, the TRSS for the V2 variant is the highest value, the same variant as seen experimentally. Thus, this variant selection is unaffected by the activity of SBs in grain #1. Taken together, it may be conjectured that either the prismatic slip in grain #1 and tensile twinning in grain #2 formed independently, a co-formation

Fig. 8. (a) SEM image reveals pair P1 with slip ↔ twin transmission across the GB after 2% uniaxial strain [15]. (b) Bicrystal model for pair P1 with a twin lamella in black. (c-d) Calculated distribution of the accumulated shear on the active prismatic system in grain #1 from pair P1 at 2% strain (c) without the twin and (d) with the twin

event, or twin lamellae in grain #2 initiated SBs in grain #1. To see if the latter is possible, we simulate the reversed transmission, in which the twins in grain #2 formed first. The result reveals intensified local stresses on the prismatic system at the twin tip inside grain #1, suggesting that a path-dependent twin-to-slip transmission is more likely

than the co-formation event.

4.4. Simulation of potential twin-to-slip transmissions

Fig. 2 shows the SEM image of pair P3 containing prismatic SBs in

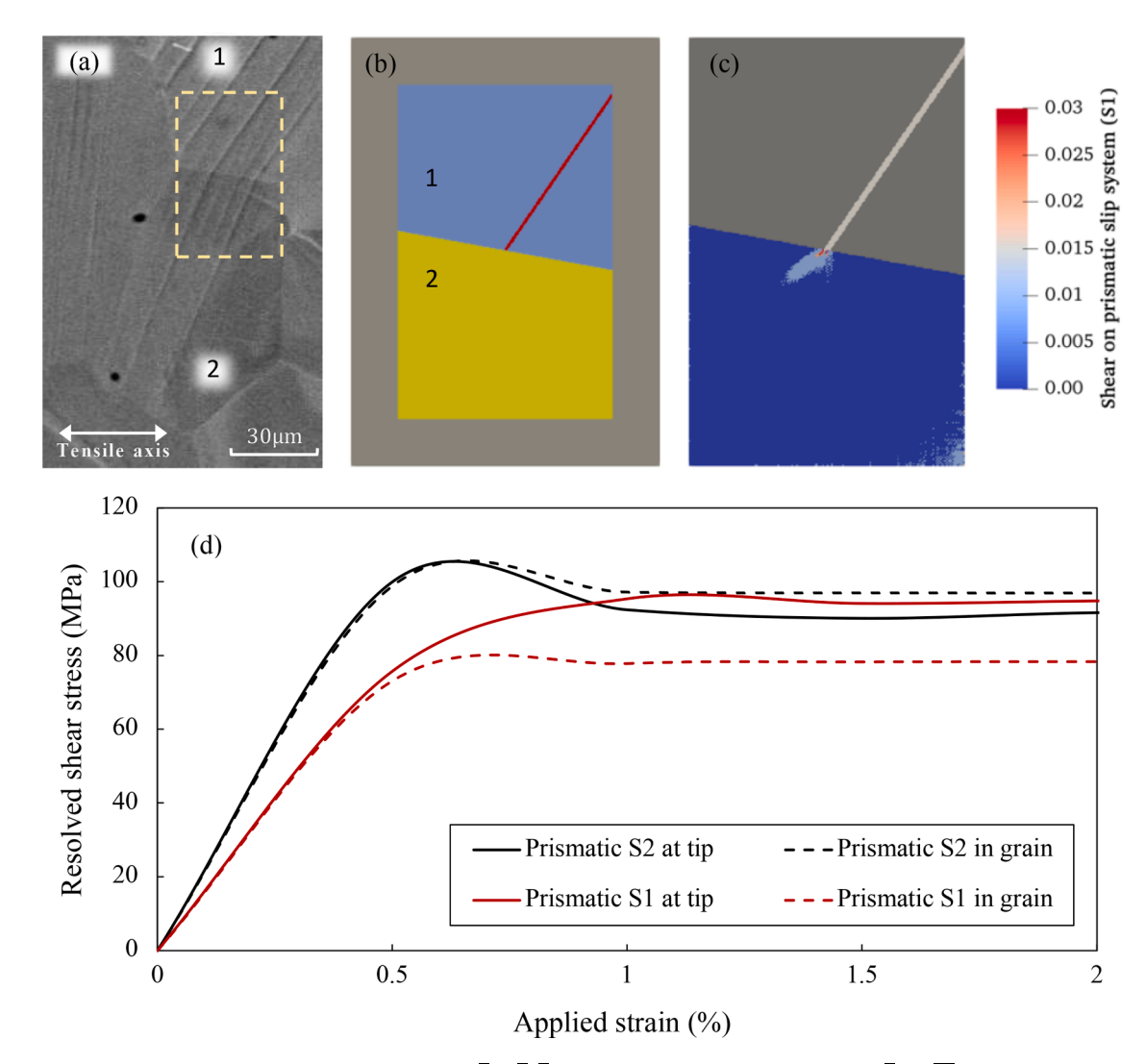


Fig. 9. (a) SEM image of pair P5 revealing transmission between $(10\overline{10})$ $[\overline{1210}]$ prismatic slip (S2) in grain #1 and $(01\overline{10})$ $[2\overline{110}]$ prismatic slip (S1) in grain #2, at 2% macroscopic strain, (b) Bicrystal model subjected to the SB constitutive law for the pair of grains shown in (a), (c) Calculated distribution of shear accumulated on the S1 prismatic system in grain #2 confirms the effect of SBs in grain #1 on the selection of system onto which they transmit in grain #2, (d) Evolution of the resolved shear stress on two prismatic slip systems denoted by "S1" and "S2", as the macroscopic strain increases. The curves are shown for both the average RSS in the SB tip zone only and in the entire grain #2.

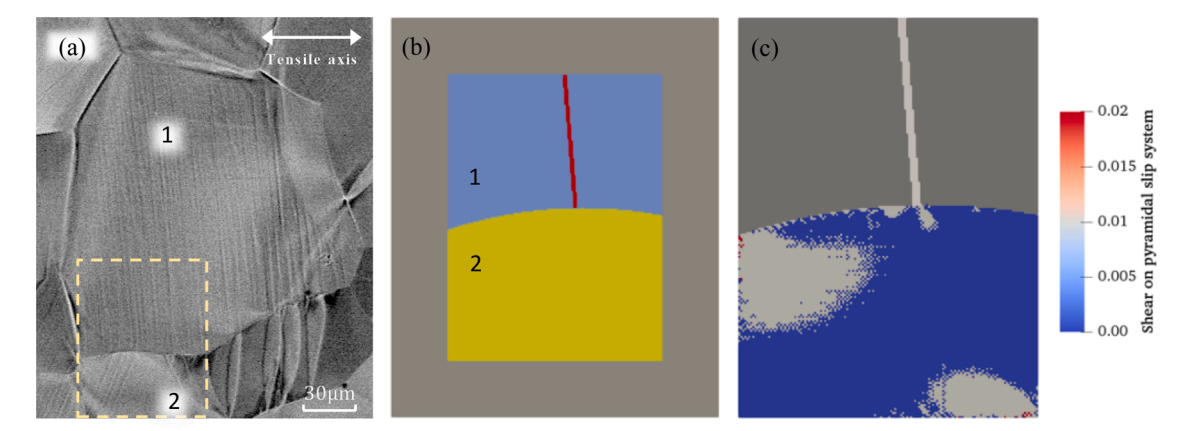


Fig. 10. (a) SEM image of pair P6 revealing transmission between $(1\overline{1}00)$ [11 $\overline{2}0$] prismatic slip (S3) in grain #1 and $(\overline{1}011)$ [2 $\overline{1}\overline{1}3$] pyramidal slip in grain #2, at 2% macroscopic strain, (b) Bicrystal model subjected to the SB constitutive law for the pair of grains shown in (a), (c) Distribution of shear accumulated on the pyramidal system in grain #2 at 4% applied strain.

grain #1 connected to two $(01\overline{1}2)$ $[0\overline{1}11]$ twin lamellae (V2) in grain #2, and the bicrystal models used to calculate stress fields in these two grains. The Schmid factor for the prismatic slip in grain #1, twin in grain #2, and the transmission factor are, respectively, $m_s = 0.47$, $m_t = 0.38$, $m^{'} = 0.88$. Fig. 6(a) presents the distribution of the TRSS for the operating twin variant (V2) in grain #2, after 2% applied strain, without a SB. Even without the SB, the TRSS is not uniformly distributed neither within grain #2 nor along its GB with grain #1. Remarkably, the location along the GB at which the TRSS is heightened, predicted by calculations, corresponds to the location of two twin lamellae formed at the GB (see Fig. 2(a)). This would suggest that twinning in grain #2 is already favored to form at the observed site in the GB without a need for SBs in grain #1.

Since the actual morphology of the GB appears to make a defining role, we show in Fig. 6(c) the contour of TRSS for the operating twin variant in grain #2 from a bicrystal model with a planar GB and without a SB in grain #1. For the planar GB, twinning in grain #2 is most likely to form at the triple junction at the top segment of the boundary, in stark contrast to experimental observations. A comparison between Fig. 6(a) and (c) implies that the morphology of the GB can influence local stress fields along the GB (through its effect on the GB shear traction) to the extent that it can control slip transmission events across the GB.

It is also possible that the SB in grain #1 participated in choosing the observed V2. Fig. 6(b) shows the V2 TRSS field due to the SB in grain #1. Perhaps counterintuitively, a local reduction occurs at the tip of the band. Not only would a SB in one grain not generate stress concentrations that promote twinning, but it would also hinder slip \rightarrow twin transmission. Evidently, SBs in grain #1 do not contribute to twinning in grain #2.

To be complete, V2 twins in grain #2 could have caused SBs in grain #1. The bicrystal model shown in Fig. 7(a) is used to calculate the resolved shear stress (RSS) fields for $(1\overline{1}00)$ [$11\overline{2}0$] prismatic slip corresponding to the observed SB. Fig. 7(b) and (c), respectively, show the contours without and with the V2 twin. Comparing these two RSS maps reveals that the twin in grain #2 maximizes the RSS in grain #1 ahead of the twin tip but lowers it elsewhere. Among all three prismatic slip variants, the active slip system, shown in Fig. 7(b, c), has the highest RSS, explaining the selection of the active slip system observed experimentally. This co-located pair likely occurred via transmission of V2 twins in grain #2 into prismatic SBs in grain #1.

Next, we present simulation results for the likely slip \leftrightarrow twin transmission event in pair P1, as shown in Fig. 8(a). High Schmid factors for the prismatic slip in grain #1 (m_s = 0.48), twin in grain #2 (m_t = 0.43), and the transmission factor (m['] = 0.93) suggest that these two mechanisms are independently favored to activate under the

macroscopic load. The bicrystal setup created to model this pair of grains is displayed in Fig. 8(b). Fig. 8(c) and (d) show the amount of shear accumulated on the prismatic slip system, the one observed experimentally, without and with the twin, respectively. The calculations suggest that under an applied strain of 2%, the prismatic slip system becomes uniformly activated within grain #1, due to the grain #1 crystal orientation with respect to loading. With the twin in grain #2, the slip activity in grain #1 escalates exclusively at the twin/GB junction.

Calculations considering the reverse path, with the SB in grain #1 and grain #2 twin free, reveal a stress concentration inside grain #2 at the SB/GB junction, for all six twin variants. Since both prismatic slip in grain #1 and $(10\overline{1}2)$ $[\overline{1}011]$ tensile twinning in grain #2 are already favored due to the parent grain orientations, the intense SBs in grain #1 and twins in grain #2 affected their location and less so their systems.

4.5. Simulation of potential slip-to-slip transmissions and blocked SBs

Other common observations include one SB or a pair of co-located SBs at GBs, signifying slip-to-slip transmission or a blocked SB. The SEM image in Fig. 9(a) shows the pair P5 with prismatic SBs in grain #1 and grain #2 correlated across a GB. In grain #1, SBs are localized on the most favorable prismatic system, S2: $(10\overline{1}0)$ $[\overline{1}2\overline{1}0]$, with a Schmid factor of $m_{s2}=0.37$. In grain #2 SBs correspond to the prismatic system S1: $(01\overline{1}0)$ $[2\overline{1}10]$, which has a lower Schmid factor of $m_{s1}=0.27$. The transmission factor associated with these two slip systems is $m^{'}=0.27$. Based on this geometric analysis alone, activation of the system S1 in grain #2 is counterintuitive since another prismatic slip system had a higher Schmid factor $(m_{s2}=0.42)$ and correspondingly higher $m^{'}$ value $(m^{'}=0.98)$ with S2 in grain #1.

To understand why slip transmission involved an unsuitably oriented slip system, two bicrystal models were simulated, each of which contains a SB in one of the grains. Fig. 9(b) shows the model with a SB in grain #1, with which the local stress fields at the band tip inside grain #2 are evaluated. Fig. 9(c) presents the distribution of shear accumulated on the active prismatic slip system in grain #2 (S1) at 2% applied strain. While the areas in the interior of the grain #2 do not accommodate any shear strain on system S1, the localized slip activity on this system at the SB tip is intense, implying that SBs in grain #2 were initiated due to prismatic SBs in grain #1. Transmission from grain #1 to grain #2 was further supported by repeating the calculation for the contrary situation, SB transmission from grain #2 to grain #1. The SB in grain #2 showed no impact on local fields at the band tip inside grain #1 and therefore this pathway is unlikely.

To compare how local stress fields encourage slip activity on these

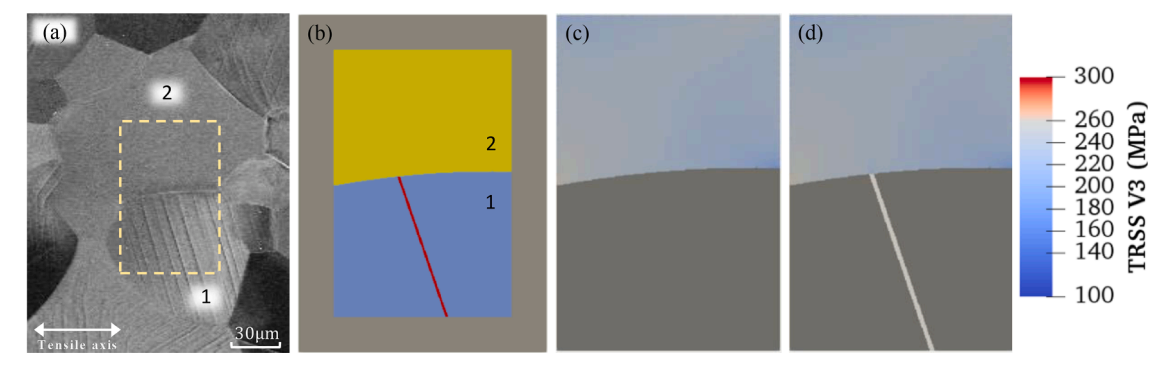


Fig. 11. (a) SEM image for pair P7 showing prismatic SBs in grain #1 blocked at the GB at 2% macroscopic strain, while some twin variants in grain #2 are perfectly aligned with the incoming slip, geometrically making the slip \rightarrow twin transmission more likely to occur, (b) Bicrystal model for pair P7 shown in (a), Calculated distribution of the twin plane resolved shear stress (TRSS) at 2% macroscopic strain for the ($\overline{1}102$) [$\overline{1}101$] twin variant (V3) that has the highest value of m $^{'}=0.98$ associated with a slip \rightarrow twin transmission, for the simulations (c) without and (d) with an intense SB in grain #1. It is noted that despite the perfect alignment between the incoming slip system and the outgoing twin variant, the band is blocked at the boundary and creates no impact on the local stress fields at the tip.

two systems in grain #2, resolved shear stress (RSS) on prismatic systems S1 and S2 are presented in Fig. 9(d), as the far-field strain increases. Notably, while the RSS for system S2 is higher than that for S1 in the interior of the grain, activity of SBs in grain #1 intensifies the RSS for system S1 at the band tip to a level higher than the local value of RSS on system S2 at the GB. In contrast to the stress states inside the grain, SBs in grain #1 encourage S1 activity, the one observed experimentally, while suppressing S2 activity at the GB.

Fig. 10 for pair P6 shows a likely transmission between $(1\overline{1}00)$ $[11\overline{2}0]$ prismatic SB in grain #1 with a Schmid factor of $m_1=0.49$ and $(\overline{1}011)$ $[2\overline{1}\overline{1}3]$ pyramidal $\langle c+a\rangle$ SB in grain #2 with a Schmid factor of $m_2=0.41$. The interesting aspect about this transmission is its extremely low $m^{'}=0.03$. The question is then why this transmission with pyramidal slip is observed instead of one involving the easier basal slip system that is more favorably oriented for activation ($m_s=0.49$) and for transmission ($m^{'}=0.65$).

To address this question, Fig. 10(c) shows the distribution of shear strain accumulated on the active pyramidal slip system in grain #2. The presented contour is obtained at 4% far-field strain since no activity at the band tip was found for any slip system at 2% strain. The calculations successfully predict activation of the hard pyramidal slip system at the band tip in grain #2, despite the very low m' value for the observed transmission. Analysis of RSS maps for the favorably oriented basal slip system further reveals that the SB in grain #1 does not promote activation of basal slip at the GB. Simulation of the reversed transmission, in which the pyramidal SB in grain #2 formed first, reveals that the local fields at the pyramidal band tip generated inside grain #1 would not favor the activation of the prismatic slip system corresponding to the observed SBs. Prismatic SBs formed first and not the other way around.

Finally, an example of blocked SBs by the GB (P7) is shown in the SEM image in Fig. 11(a), where intense prismatic SBs in grain #1 were not transmitted into grain #2. The bicrystal model used to study stress fields at the band tip is also shown in Fig. 11(b). While grain #2 experienced homogeneous deformation, or no deformation at all, calculations indicate multiple slip and twinning modes in this grain that are favored by the far-field loading orientation and are well-aligned with prismatic SBs in grain #1. The most likely slip system in grain #2 for a slip-to-slip transmission is $(01\overline{1}1)$ $[1\overline{2}13]$ pyramidal slip with $m_s = 0.49$ and m' = 0.74, while the most likely twin variant for a slip-to-twin transmission is $(\overline{1}102)$ $[1\overline{1}01]$ twin variant (V3) with $m_t = 0.46$ and m' =0.98. Calculations reveal no intensifying or weakening effect from the SB in grain #1 on the local stress fields at the GB for any slip system or twin variant. Contours of the TRSS for the $(\overline{1}102)$ $[1\overline{1}01]$ twin variant (V3) at 2% macroscopic strain are shown in Fig. 11(c) and (d), respectively, for models without and with a SB in grain #1. These explain why the SBs did not promote twin variant V3 in the neighboring grain #2.

The resolved shear stresses for all slip and twinning modes at any point inside grain #2 are below their applicable critical value. Consequently, the accumulated shear strain on all slip systems is zero, indicating that grain #2 accommodated no strain at all. Despite high values of $m^{'}$ and m_{s} , not all SBs will transmit SBs or trigger twins across a boundary and those that are blocked can be identified because they do not generate driving forces.

5. Discussion

It was previously reported in [84] that the contribution of the GB shear traction to the overall resolved shear stress developed at the GB can affect whether the GB assists or inhibits the emission of dislocations at the GB, a phenomenon directly associated with slip transmission across the GB. It can be envisioned that GB morphology could be included in GB engineering to control deformation mechanisms within the grains and inhibit or promote their transmissions across the GBs. As suggested by the TRSS fields in Fig. 6(c, e), a curved GB, especially the segments of it that make a 45° angle with the loading axis, promotes twin formation from the boundary more than a planar boundary would. This finding is in agreement with the effect of GB orientation on slip activity in CP-Ti reported in an experimental study [30], where it was found that a change in the orientation of the GB with respect to loading direction necessitates the activation of secondary slip systems in proximity to the grain boundaries.

It is also demonstrated here that GB/band junction stress fields can help to identify the transmission path, that is, which mechanism initiated the transmission and which one completed it. Contrary to previous speculations that most twins in the studied CP-Ti sample were formed via a slip-stimulated twin nucleation mechanism [15], we reveal the reverse, in which some of the co-located slip and twin bands in CP-Ti manifest first as twins, which then stimulated a SB in the grain neighbor. Table 5 summarizes simulation and experimental results for each studied pair. Depending on the calculated stress fields around the co-located pairs, each transmission case is classified as one of the followings; $S \rightarrow T$ for slip-to-twin transmission, $T \rightarrow S$ for twin-to-slip transmission, $S \rightarrow S$ for slip-to-slip transmission, and $S \dashv 0$ for SBs that are blocked at the GB. Many studies have reported various effective techniques, such as grain size refinement and adding solid solution or precipitates, for inhibiting twinning in titanium [86-90]. Thus, the direction of the transmission path taken can have implications on the effectiveness of such techniques. Particularly, if most SBs are activated by the twin bands, inhibiting the formation of twins may cause reduced formability in the material associated with the lower extent of slip.

Several cases presented here demonstrate that simple geometric parameters, such as Schmid factor and $m^{'}$, that have been widely used to

Iwin variants observed in transmission instances, the Schmid factors for the incoming and outgoing systems, and the geometric factor m' associated with the transmission. To compare simulation results with experimental observations, the deformation mode in the neighbor with the highest RSS value and the slip/twin band effect on the local stress state at the band tip are also presented for each pair. The slip mode where intense SBs are detected is prismatic slip (except for P6). See Table 4 for crystallographic information about different variants of prismatic slip and tensile twinning.

	Pair	Observed SB	SB	Observed	Observed twin / SB	`E	Deformation mode with highest RSS	SB effect on stress at	Prismatic variant with highest RSS Twin/SB effect on stress at	Twin/SB effect on stress at	Transmission
		Prismatic variant	m ^s	variant	m _t or m _s		at the tip	the tip	at the tip	the tip	classification
1	P1	2	0.48	1	0.43	0.94	6,3	Intensifying	3,2	Intensifying	T → S
L	P2	2	0.44	9	0.23	0.89	9	Intensifying	I	I	$S \to T$
	Ь3	က	0.47	2	0.38	0.88	1,4	Weakening	3,1	Intensifying	$T \to S$
	Ъ4	2	0.50	2	0.39	0.79	2,5	No effect	2,1	Intensifying	$T \to S$
1	P5	2	0.37	1	0.27	0.27	1,2	Intensifying	2,1	No effect	$S2 \rightarrow S1$
S	P6	3	0.49	$\langle c+a \rangle^a$	0.41	0.03	<c+a>a</c+a>	Intensifying	3	No effect	S3 $\rightarrow \langle c+a \rangle$
0 ⊢ S	Ь7	3	0.49	1	I	ı	ı	No effect	1	1	$S \dashv 0$

Observed slip mode is $(\overline{1}011)$ $[2\overline{1}\overline{1}3]$ $\langle c+a \rangle$ pyramidal slip system.

forecast active deformation mechanisms and their potential transmission across boundaries are not consistently reliable. First, while undoubtedly beneficial for quickly identifying the most favorable pair for transmission, they do not identify whether this transmission happens in the first place. Second, they clearly do not account for differences in deformation mechanisms at the GB junction from the rest of the grain or for the GB morphology. This conclusion supports several experimental studies that have reported many instances in which m' was not effective in explaining why the observed transmission occurred or a potential transmission did not [25,26,36]. While requiring more computation, an intragranular stress-based criterion, such as the one presented in this work, provides a better prediction and accounts for these features. In fact, it has been established that, in addition to good alignment between two slip systems, as indicated by m', the outgoing system needs to have a sufficiently large resolved shear stress level from the dislocation pile-up stress field before a transmission can occur [91]. While the notion is acceptable, identifying the variables that affect these local RSS has not been straightforward. As demonstrated here, these driving stresses are localized and depend on the properties of both the band that impinges on the GB and the GB itself. For instance, local stresses explain the activation of a prismatic slip system despite its low Schmid factor and low m', in favor of other prismatic systems with higher values of m_s and m'. Similarly, local stresses developing at the GB/SB junction explain the observed transmission to a hard pyramidal $\langle c+a \rangle$ slip system despite its nearly zero m'. Last, local stresses explain why a SB would become blocked despite many potential pathways with high m'.

Finally, we remark that many current constitutive models for HCP materials that deform by slip and twinning do not consider the exchange of deformation mechanisms into and out of a grain from its neighborhood. Most modeling techniques predict deformation mechanisms in the grain based on the stress field calculated using grain properties and constraints of neighboring grains [66,92,93]. Three-dimensional, spatially resolved crystal plasticity models, for instance, consider the influence of the stress and deformation response of grain neighborhoods under compatibility constraints [32,94-96]. Local stress fields can be generated at the GBs or triple junctions that differ from the stress field in the interior of the grain as a result. Invariably, the slip and twin activity and orientations in these regions would differ as well [97–100]. Yet still, in these models, deformation mechanisms are not transmitted, and the dependence on the neighborhood is indirect. Analysis of local band/GB junctions of many co-located pairs studied here shows that the slip or twin happened in one grain only because it was passed from its neighboring grain. The event in Fig. 4, for instance, exemplifies tensile twins activated in the neighboring grain caused by stress concentrations from the SBs in the parent grain. The tensile twins superseded prismatic slip, which would have been expected or predicted in that grain based on its properties. While including deformation "fluxes" in such models is numerically challenging, a part of the roadblock has been the lack in understanding the direction of transmission and which slip system or twin variant are involved. The present results provide guidance on selecting the participating direction and crystallographic pathway.

6. Conclusions

Consistent with the report previously published in [15] on a part of the deformed microstructure, experimental observations from the newly presented data in this work show that the plastic deformation in CP-Ti is mainly realized via strong localized crystallographic bands, either $\{10\overline{1}2\}~\langle\overline{1}011\rangle$ twins or prismatic SBs. These localized bands are typically seen to intersect at the parent grain boundaries, having initiated or terminated there. In some instances, SBs or twins terminating in the interior of the grain were also observed. In either case, many GBs show a clear correlation in location for slip/twin bands on two sides of the boundary, forming co-located pairs. What is not clear from SEM images, however, is whether these co-located pairs were achieved via a

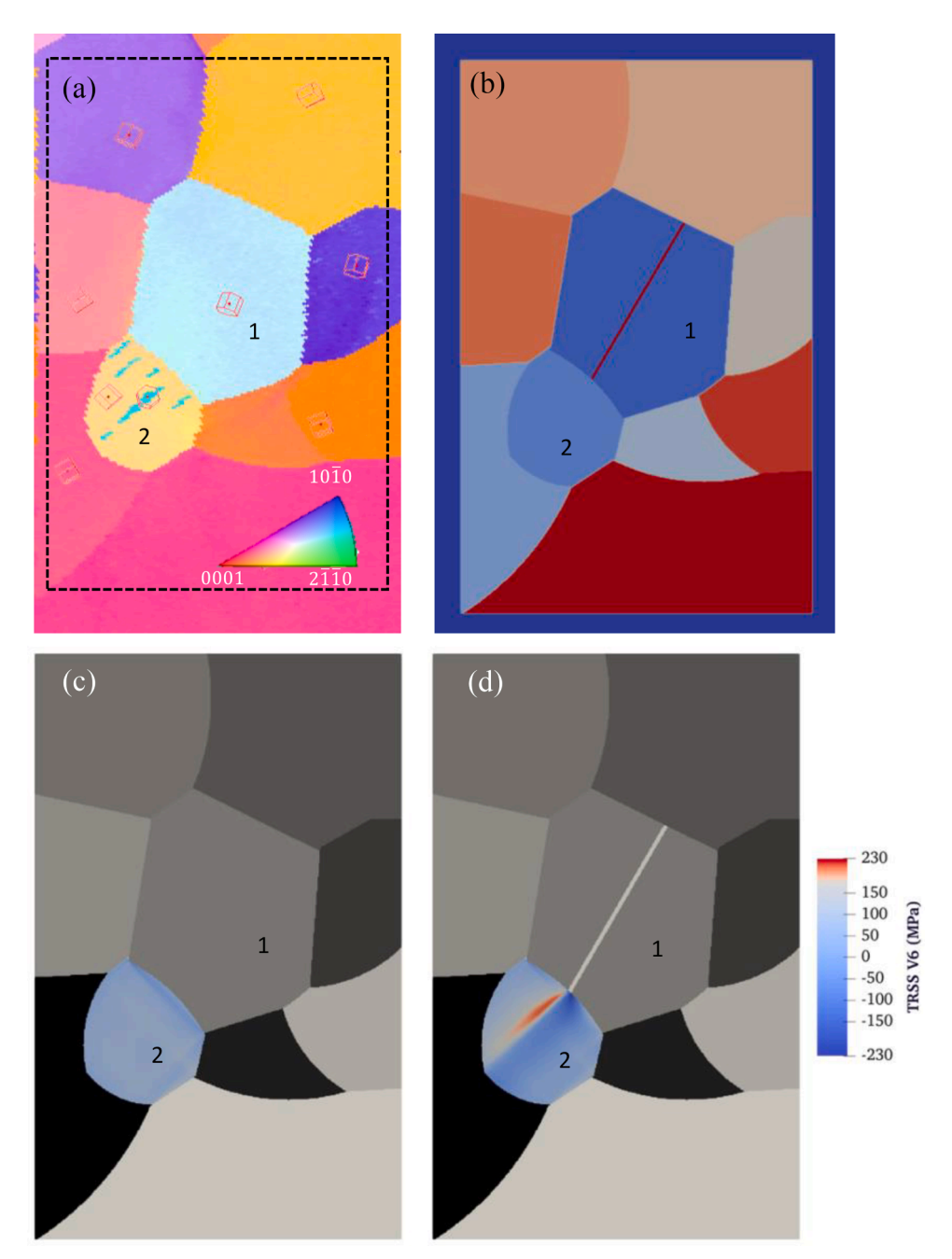


Fig. A.1. (a) EBSD map of grain #1 (slip banded) and grain #2 (twinned) and their neighboring grains. (b) The microstructure model created for CPFFT calculation of 10 grains contained in the dashed box in (a). (c, d) Calculated field at 2% macroscopic strain of the twin plane resolved shear stress (TRSS) for the $(1\overline{1}02)$ [$\overline{1}101$] tensile twin variant (V6) (c) without and (d) with an intense slip band in grain #1.

directional, path-dependent transmission or independently via a co-formation event. To address this question, we present a crystal plasticity fast Fourier transform model that uniquely treats both discrete SBs and twin lamellae. Unlike most modeling techniques that predict deformation in each grain based on the grain properties, the present model directly incorporates grain neighbor properties into the prediction of deformation mechanisms in the parent grain. The model is applied to bicrystal unit cells that replicated a pair of grain with transmission from SEM images. Studying local stress field caused by a slip or twin band at the GB/band junction, we investigate the propensity for a new slip/twin band to form in the grain neighbor, and hence identify the transmission path taken. We show that the local stress field calculated by discrete slip and twin band model can determine not only if a transmission has occurred in an observed co-located pair, but also the

direction of the transmission, an insight that geometric criteria, such as $m^{'},\,\,$ cannot provide. We further reveal that retaining the actual morphology of the GB when modeling a set of grains can heavily influence local stress fields developed near the boundary, and consequently, the slip/twin transmission across the GB. Such influence ensues from the effect of GB morphology on the intensity of the sudden disruption in the GB shear traction that occurs at the discrete slip or twin band/GB junction and contributes to the local back-stress and stress concentration developed on either side of the boundary.

Declaration of Competing Interest

The authors declare that they have no known competing financial interests or personal relationships that could have appeared to influence

the work reported in this paper.

Acknowledgments

B. A. and I.J.B. acknowledge financial support from the National Science Foundation (NSF CMMI-2051390). MAK acknowledges the financial support from the U.S. Dept. of Energy, Office of Basic Energy Sciences Project FWP 06SCPE401. Experimental data used for this research was funded by a Materials World Network grant from the National Science Foundation (T.R. Bieler, M.A. Crimp, Grant No. DMR-0710570) and Deutsche Forschungsgemeinschaft (P. Eisenlohr, Grant No. EI 681/2-1). Use was made of computational facilities purchased with funds from the National Science Foundation (CNS-1725797) and administered by the Center for Scientific Computing (CSC). The CSC is supported by the California NanoSystems Institute and the Materials Research Science and Engineering Center (MRSEC; NSF DMR 1720256) at UC Santa Barbara.

Appendix

To investigate how an active SB/twin lamella in one grain influences the local stress field in the neighboring grain, we model a discrete SB/twin lamella within a bicrystal setup that consists of only the two grains of interest. We do not spatially resolve the stress field in more neighboring grains, relying on the assumption that the local stress field within and around the tip of the slip band or the twin lamella outweighs the stress heterogeneity due to the presence of the next nearest neighboring grains. To check this assumption, we select the pair P2 and repeat our calculations, this time on a model microstructure that contains more neighboring grains. Fig. A.1(a) and (b) respectively, shows the EBSD map of pair P2 and its neighboring grains, and the model microstructure we created for modeling this grain aggregate.

Calculated at 2% applied strain, Fig. A.1(c) and (d) shows the distribution of the resolved shear stress for the experimentally observed twin variant in grain #2, for the extended model microstructure, respectively, without and with a SB modeled in grain #1. A comparison between Figs. A.1(c) and 4(c) reveals that the direct interaction of neighboring grains slightly changes the stress distribution in grain #2 in the SB-free models. When a slip band is modeled in grain #1, the local stress distribution in grain #2 is heavily influenced by the slip bandinduced stress concentration ahead of the band near the grain boundary, as indicated by comparing Figs. A.1(d) and 4(d). Therefore, the local stress field at the band tip completely outweighs any stress heterogeneities due to the constraint effects from more neighboring grains. This validates our assumption that the local stress fields developed ahead of localized slip/twin bands heavily influence the selection of slip system or twin variant at the GB within the neighboring grain, onto which the transmission is likely to occur. It further demonstrates that resolving more of the neighboring grains does not affect the conclusions made in this work.

References

- R.R. Boyer, An overview on the use of titanium in the aerospace industry, Mater. Sci. Eng. A 213 (1–2) (1996) 103–114.
- [2] M. Niinomi, Mechanical properties of biomedical titanium alloys, Mater. Sci. Eng. A 243 (1–2) (1998) 231–236.
- [3] M. Koike, H. Fujii, The corrosion resistance of pure titanium in organic acids, Biomaterials 22 (21) (2001) 2931–2936.
- [4] X. Liu, P.K. Chu, C. Ding, Surface modification of titanium, titanium alloys, and related materials for biomedical applications, Mater. Sci. Eng. R Rep. 47 (3–4) (2004) 49–121.
- [5] I. Inagaki, T. Takechi, Y. Shirai, N. Ariyasu, Application and features of titanium for the aerospace industry, Nippon Steel Sumitomo Met. Tech. Rep. 106 (106) (2014) 22-27
- [6] N. Yi, T. Hama, A. Kobuki, H. Fujimoto, H. Takuda, Anisotropic deformation behavior under various strain paths in commercially pure titanium grade 1 and grade 2 sheets, Mater. Sci. Eng. A 655 (2016) 70–85.

[7] M.E. Nixon, O. Cazacu, R.A. Lebensohn, Anisotropic response of high-purity α-titanium: experimental characterization and constitutive modeling, Int. J. Plast. 26 (4) (2010) 516–532.

- [8] L. Wang, R. Barabash, T. Bieler, W. Liu, P. Eisenlohr, Study of \$\$\{11\bar {2} 1\} \$\$ twinning in α-Ti by EBSD and laue microdiffraction, Metall. Mater. Trans. A 44 (8) (2013) 3664–3674.
- [9] S. Nemat-Nasser, W. Guo, J. Cheng, Mechanical properties and deformation mechanisms of a commercially pure titanium, Acta Mater. 47 (13) (1999) 3705–3720
- [10] D.H. Shin, I. Kim, J. Kim, Deformation mechanisms of pure Ti during equal channel angular pressing, Met. Mater. Int. 8 (6) (2002) 513–518.
- [11] K.E.K. Amouzou, T. Richeton, A. Roth, M. Lebyodkin, T. Lebedkina, Micromechanical modeling of hardening mechanisms in commercially pure α-titanium in tensile condition, Int. J. Plast. 80 (2016) 222–240.
- [12] J. Ren, Q. Wang, X. Lu, W. Liu, P. Zhang, X. Zhang, Effect of oxygen content on active deformation systems in pure titanium polycrystals, Mater. Sci. Eng. A 731 (2018) 530–538.
- [13] B. Barkia, V. Doquet, J.P. Couzinie, I. Guillot, E. Héripré, *In situ* monitoring of the deformation mechanisms in titanium with different oxygen contents, Mater. Sci. Eng. A 636 (2015) 91–102.
- [14] N. Benmhenni, S. Bouvier, R. Brenner, T. Chauveau, B. Bacroix, Micromechanical modelling of monotonic loading of CP α-Ti: correlation between macroscopic and microscopic behaviour, Mater. Sci. Eng. A 573 (2013) 222–233.
- [15] L. Wang, Y. Yang, P. Eisenlohr, T. Bieler, M. Crimp, D. Mason, Twin nucleation by slip transfer across grain boundaries in commercial purity titanium, Metall. Mater. Trans. A 41 (2) (2010) 421.
- [16] T.R. Bieler, L. Wang, A.J. Beaudoin, P. Kenesei, U. Lienert, *In situ* characterization of twin nucleation in pure Ti using 3D-XRD, Metall. Mater. Trans. A 45 (1) (2014)
- [17] M.A. Kumar, M. Wroński, R.J. McCabe, L. Capolungo, K. Wierzbanowski, C. N. Tomé, Role of microstructure on twin nucleation and growth in HCP titanium: a statistical study, Acta Mater. 148 (2018) 123–132.
- [18] X. Guan, L. Lu, S. Luo, D. Fan, *In situ* observations of detwinning and strain localization in pure titanium, Mater. Sci. Eng. A 813 (2021), 141073.
- [19] Z. Zhang, Z. Wang, Dependence of intergranular fatigue cracking on the interactions of persistent slip bands with grain boundaries, Acta Mater. 51 (2) (2003) 347–364.
- [20] K.S. Chan, D.L. Davidson, Evidence of void nucleation and growth on planar slip bands in a Nb-Cr-Ti alloy, Metall. Mater. Trans. A 30 (3) (1999) 579–585.
- [21] M.P. Echlin, J.C. Stinville, V.M. Miller, W.C. Lenthe, T.M. Pollock, Incipient slip and long range plastic strain localization in microtextured Ti-6Al-4V titanium, Acta Mater. 114 (2016) 164–175.
- [22] M.D. Sangid, H.J. Maier, H. Sehitoglu, The role of grain boundaries on fatigue crack initiation—an energy approach, Int. J. Plast. 27 (5) (2011) 801–821.
- [23] C. Guo, R. Xin, C. Ding, B. Song, Q. Liu, Understanding of variant selection and twin patterns in compressed Mg alloy sheets via combined analysis of Schmid factor and strain compatibility factor, Mater. Sci. Eng. A 609 (2014) 92–101.
- [24] D. Culbertson, Q. Yu, Y. Jiang, *In situ* observation of cross-grain twin pair
- formation in pure magnesium, Philos. Mag. Lett. 98 (4) (2018) 139–146.
 Y. Guo, T. Britton, A. Wilkinson, Slip band–grain boundary interactions in commercial-purity titanium, Acta Mater. 76 (2014) 1–12.
- [26] Y. Guo, D.M. Collins, E. Tarleton, F. Hofmann, A.J. Wilkinson, T.B. Britton, Dislocation density distribution at slip band-grain boundary intersections, Acta Mater. 182 (2020) 172–183.
- [27] Y. Su, S. Han, P. Eisenlohr, M.A. Crimp, Predicting shear transmission across grain boundaries with an iterative stress relief model, Acta Mater. (2021), 116992.
- [28] S. Han, P. Eisenlohr, M.A. Crimp, ECCI based characterization of dislocation shear in polycrystalline arrays during heterogeneous deformation of commercially pure titanium, Mater. Charact. 142 (2018) 504–514.
- [29] L. Wang, P. Eisenlohr, Y. Yang, T. Bieler, M. Crimp, Nucleation of paired twins at grain boundaries in titanium, Scr. Mater. 63 (8) (2010) 827–830.
- [30] S. Han, M.A. Crimp, ECCI analysis of shear accommodations at grain boundaries in commercially pure alpha titanium, Int. J. Plast. 131 (2020), 102731.
- [31] Y. Yang, L. Wang, T. Bieler, P. Eisenlohr, M. Crimp, Quantitative atomic force microscopy characterization and crystal plasticity finite element modeling of heterogeneous deformation in commercial purity titanium, Metall. Mater. Trans. A 42 (3) (2011) 636–644.
- [32] L. Wang, R. Barabash, Y. Yang, T. Bieler, M. Crimp, P. Eisenlohr, W. Liu, G.E. Ice, Experimental characterization and crystal plasticity modeling of heterogeneous deformation in polycrystalline α-Ti, Metall. Mater. Trans. A 42 (3) (2011) 626–635.
- [33] J. Luster, M. Morris, Compatibility of deformation in two-phase Ti-Al alloys: dependence on microstructure and orientation relationships, Metall. Mater. Trans. A 26 (7) (1995) 1745–1756.
- [34] T. Bieler, P. Eisenlohr, C. Zhang, H. Phukan, M. Crimp, Grain boundaries and interfaces in slip transfer, Current Opinion in Solid State and, Mater. Sci. 18 (4) (2014) 212–226.
- [35] M.A. Kumar, I.J. Beyerlein, R.J. McCabe, C.N. Tome, Grain neighbour effects on twin transmission in hexagonal close-packed materials, Nat. Commun. 7 (1) (2016) 1–9.
- [36] B. Zhou, L. Wang, P. Jin, H. Jia, H.J. Roven, X. Zeng, Y. Li, Revealing slip-induced extension twinning behaviors dominated by micro deformation in a magnesium alloy, Int. J. Plast. 128 (2020), 102669.
- [37] J. Hirth, J. Wang, C. Tomé, Disconnections and other defects associated with twin interfaces, Prog. Mater Sci. 83 (2016) 417–471.

- [38] S. Chen, Q. Yu, The role of low angle grain boundary in deformation of titanium and its size effect, Scr. Mater. 163 (2019) 148–151.
- [39] Z. Zheng, D.S. Balint, F.P. Dunne, Investigation of slip transfer across HCP grain boundaries with application to cold dwell facet fatigue, Acta Mater. 127 (2017) 43–53.
- [40] Z. Tong, L. Wang, G. Zhu, X. Zeng, Predicting twin nucleation in a polycrystalline Mg alloy using machine learning methods, Metall. Mater. Trans. A 50 (12) (2019) 5543–5560.
- [41] Y. Brechet, G. Canova, L. Kubin, Strain softening, slip localization and propagation: from simulations to continuum modelling, Acta Mater. 44 (11) (1996) 4261–4271.
- [42] Y. Estrin, L. Kubin, Local strain hardening and nonuniformity of plastic deformation, Acta Metall. 34 (12) (1986) 2455–2464.
- [43] N.R. Barton, A. Arsenlis, J. Marian, A polycrystal plasticity model of strain localization in irradiated iron, J. Mech. Phys. Solids 61 (2) (2013) 341–351.
- [44] T. Erinosho, F. Dunne, Strain localization and failure in irradiated zircaloy with crystal plasticity, Int. J. Plast. 71 (2015) 170–194.
- [45] J. Hure, S. El Shawish, L. Cizelj, B. Tanguy, Intergranular stress distributions in polycrystalline aggregates of irradiated stainless steel, J. Nucl. Mater. 476 (2016) 231–242.
- [46] A. Patra, D.L. McDowell, Crystal plasticity-based constitutive modelling of irradiated bcc structures, Philos. Mag. 92 (7) (2012) 861–887.
- [47] A. Patra, D.L. McDowell, Crystal plasticity investigation of the microstructural factors influencing dislocation channeling in a model irradiated bcc material, Acta Mater. 110 (2016) 364–376.
- [48] M. Zhang, F. Bridier, P. Villechaise, J. Mendez, D. McDowell, Simulation of slip band evolution in duplex Ti-6Al-4V, Acta Mater. 58 (3) (2010) 1087–1096.
- [49] S. Forest, Modeling slip, kink and shear banding in classical and generalized single crystal plasticity, Acta Mater. 46 (9) (1998) 3265–3281.
- [50] S. Keshavarz, S. Ghosh, Hierarchical crystal plasticity FE model for nickel-based superalloys: sub-grain microstructures to polycrystalline aggregates, Int. J. Solids Struct. 55 (2015) 17–31.
- [51] Y. Tadano, Y. Yoshihara, S. Hagihara, A crystal plasticity modeling considering volume fraction of deformation twinning, Int. J. Plast. 84 (2016) 88–101.
- [52] N. Grilli, A.C. Cocks, E. Tarleton, A phase field model for the growth and characteristic thickness of deformation-induced twins, J. Mech. Phys. Solids 143 (2020), 104061.
- [53] S. Hu, C.H. Henager Jr, L. Chen, Simulations of stress-induced twinning and detwinning: a phase field model, Acta Mater. 58 (19) (2010) 6554–6564.
- [54] J.D. Clayton, J. Knap, A phase field model of deformation twinning: nonlinear theory and numerical simulations, Phys. D 240 (9–10) (2011) 841–858.
- [55] C. Liu, P. Shanthraj, M. Diehl, F. Roters, S. Dong, J. Dong, W. Ding, D. Raabe, An integrated crystal plasticity-phase field model for spatially resolved twin nucleation, propagation, and growth in hexagonal materials, Int. J. Plast. 106 (2018) 203–227.
- [56] B. Ahmadikia, M.A. Kumar, I.J. Beyerlein, Effect of neighboring grain orientation on strain localization in slip bands in HCP materials, Int. J. Plast. (2021), 103026.
- [57] A. Marano, L. Gélébart, S. Forest, Intragranular localization induced by softening crystal plasticity: analysis of slip and kink bands localization modes from high resolution FFT-simulations results, Acta Mater. 175 (2019) 262–275.
- [58] A. Marano, L. Gélébart, Non-linear composite voxels for FFT-based explicit modeling of slip bands: application to basal channeling in irradiated Zr alloys, Int. J. Solids Struct. (2020).
- [59] M.A. Kumar, I.J. Beyerlein, Influence of plastic properties on the grain size effect on twinning in Ti and Mg, Mater. Sci. Eng. A 771 (2020), 138644.
- [60] M.A. Kumar, I.J. Beyerlein, Local microstructure and micromechanical stress evolution during deformation twinning in hexagonal polycrystals, J. Mater. Res. 35 (3) (2020) 217–241.
- [61] M.A. Kumar, L. Capolungo, R. McCabe, C. Tomé, Characterizing the role of adjoining twins at grain boundaries in hexagonal close packed materials, Sci. Rep. 9 (1) (2019) 1–10.
- [62] B. Ahmadikia, O. Paraskevas, W. Van Hyning, J. Hestroffer, I. Beyerlein, C. Thrampoulidis, Data-driven texture design for nearly-isotropic elastic and plastic properties in titanium-based materials, 2022, https://doi.org/10.21203/ rs.3.rs-1848053/v1.
- [63] Y. Sun, K. Zhou, H. Qiao, R. Xin, H. Wang, P. Wu, Crystal plasticity-based finite element modeling of twin transmission across grain boundaries in magnesium, Mater. Today Commun. 30 (2022), 102998.
- [64] M.A. Kumar, I.J. Beyerlein, R.A. Lebensohn, C.N. Tome, Role of alloying elements on twin growth and twin transmission in magnesium alloys, Mater. Sci. Eng. A 706 (2017) 295–303.
- [65] B. Wagenknecht, D. Libiran, S. Poon, K. Sztykiel, In-Situ Four-Point Bending Apparatus for Scanning Electron Micro-Scopes, Senior Design Project, Mechanical Engineering, Michigan State University, 2008.
- [66] R.A. Lebensohn, A.K. Kanjarla, P. Eisenlohr, An elasto-viscoplastic formulation based on fast Fourier transforms for the prediction of micromechanical fields in polycrystalline materials, Int. J. Plast. 32 (2012) 59–69.
- [67] M.A. Kumar, I.J. Beyerlein, C.N. Tomé, Effect of local stress fields on twin characteristics in HCP metals, Acta Mater. 116 (2016) 143–154.
- [68] M. Arul Kumar, I.J. Beyerlein, C.N. Tome, Grain size constraints on twin expansion in hexagonal close packed crystals, J. Appl. Phys. 120 (15) (2016), 155105.
- [69] M. Bapna, M. Meshii, Deformation of quench-hardened gold single crystals, Mater. Sci. Eng. 16 (1–2) (1974) 181–191.

[70] T. Byun, N. Hashimoto, K. Farrell, E. Lee, Characteristics of microscopic strain localization in irradiated 316 stainless steels and pure vanadium, J. Nucl. Mater. 349 (3) (2006) 251–264.

- [71] M. Lai, C.C. Tasan, D. Raabe, Deformation mechanism of ω -enriched Ti–Nb-based gum metal: dislocation channeling and deformation induced ω - β transformation, Acta Mater. 100 (2015) 290–300.
- [72] T. Mori, M. Meshii, Plastic deformation of quench-hardened aluminum single crystals, Acta Metall. 17 (2) (1969) 167–175.
- [73] T. Neeraj, D.H. Hou, G. Daehn, M. Mills, Phenomenological and microstructural analysis of room temperature creep in titanium alloys, Acta Mater. 48 (6) (2000) 1225–1238.
- [74] J. Sharp, Correlation between cleared channels and surface slip steps in neutron irradiated copper crystals, Radiat. Eff. 14 (1–2) (1972) 71–75.
- [75] D. Ulmer, C. Altstetter, Hydrogen-induced strain localization and failure of austenitic stainless steels at high hydrogen concentrations, Acta Metall. Mater. 39 (6) (1991) 1237–1248.
- [76] L. Xiao, Y. Umakoshi, Cyclic deformation behaviour and dislocation structure of Ti-5 at % Al single crystals oriented for double prism slip, Philos. Mag. A 82 (12) (2002) 2379–2396.
- [77] L. Xiao, Y. Umakoshi, Cyclic deformation behaviour and saturation bundle structure in Ti-5 at.% Al single crystals deforming by single prism slip, Philos. Mag. 83 (30) (2003) 3407–3426.
- [78] L. Xiao, Y. Umakoshi, Cyclic deformation behavior and dislocation structure of Ti-2 at. Pct Al single crystals oriented for double prism slip, Metall. Mater. Trans. A 35 (9) (2004) 2845–2852.
- [79] X. Xiao, D. Song, J. Xue, H. Chu, H. Duan, A size-dependent tensorial plasticity model for FCC single crystal with irradiation, Int. J. Plast. 65 (2015) 152–167.
- [80] C.M. Kube, Elastic anisotropy of crystals, AIP Adv. 6 (9) (2016), 095209.
- [81] L. Wang, Z. Zheng, H. Phukan, P. Kenesei, J.S. Park, J. Lind, R. Suter, T.R. Bieler, Direct measurement of critical resolved shear stress of prismatic and basal slip in polycrystalline Ti using high energy X-ray diffraction microscopy, Acta Mater. 132 (2017) 598–610.
- [82] G. Simmons, H. Wang, A Handbook of Single Crystal Elastic Constants and Calculated Aggregate Properties, MIT Press, Cambridge, MA, USA, 1971.
- [83] M. Yoo, Slip, twinning, and fracture in hexagonal close-packed metals, Metall. Trans. A 12 (3) (1981) 409–418.
- [84] R. Li, H.B. Chew, Grain boundary traction signatures: quantifying the asymmetrical dislocation emission processes under tension and compression, J. Mech. Phys. Solids 103 (2017) 142–154.
- [85] Y.B. Chun, S.H. Yu, S. Semiatin, S.K. Hwang, Effect of deformation twinning on microstructure and texture evolution during cold rolling of CP-titanium, Mater. Sci. Eng. A 398 (1–2) (2005) 209–219.
- [86] B. Wang, H. Liu, Y. Zhang, B. Zhou, L. Deng, C. Wang, J. Chen, Y. Zhang, Effect of grain size on twinning behavior of pure titanium at room temperature, Mater. Sci. Eng. A 827 (2021), 142060.
- [87] J. Sun, P. Trimby, F. Yan, X. Liao, N. Tao, J. Wang, Grain size effect on deformation twinning propensity in ultrafine-grained hexagonal close-packed titanium, Scr. Mater. 69 (5) (2013) 428–431.
- [88] A. Ghaderi, M.R. Barnett, Sensitivity of deformation twinning to grain size in titanium and magnesium. Acta Mater. 59 (20) (2011) 7824–7839.
- [89] E. Cerreta, G.G. Iii, A. Lawson, T. Mason, C. Morris, The influence of oxygen content on the α to ω phase transformation and shock hardening of titanium, J. Appl. Phys. 100 (1) (2006), 013530.
- [90] Y. Xu, B. Zhang, Effects of hydrogen as a solid solution element on the deformation behavior of a near-alpha titanium alloy, Mater. Sci. Eng. A 815 (2021), 141269.
- [91] T. Lee, I. Robertson, H. Birnbaum, TEM in situ deformation study of the interaction of lattice dislocations with grain boundaries in metals, Philos. Mag. A 62 (1) (1990) 131–153.
- [92] F. Roters, P. Eisenlohr, L. Hantcherli, D.D. Tjahjanto, T.R. Bieler, D. Raabe, Overview of constitutive laws, kinematics, homogenization and multiscale methods in crystal plasticity finite-element modeling: theory, experiments, applications, Acta Mater. 58 (4) (2010) 1152–1211.
- [93] J. Clayton, J. Knap, Phase field modeling of directional fracture in anisotropic polycrystals, Comput. Mater. Sci. 98 (2015) 158–169.
- [94] H. Abdolvand, J. Wright, A.J. Wilkinson, Strong grain neighbour effects in polycrystals, Nat. Commun. 9 (1) (2018) 1–11.
- [95] C. Zhang, H. Li, P. Eisenlohr, W. Liu, C. Boehlert, M. Crimp, T. Bieler, Effect of realistic 3D microstructure in crystal plasticity finite element analysis of polycrystalline Ti-5Al-2.5 Sn, Int. J. Plast. 69 (2015) 21–35.
- [96] S. Sun, V. Sundararaghavan, A probabilistic crystal plasticity model for modeling grain shape effects based on slip geometry, Acta Mater. 60 (13–14) (2012) 5233–5244.
- [97] Z. Zhang, D. Lunt, H. Abdolvand, A.J. Wilkinson, M. Preuss, F.P. Dunne, Quantitative investigation of micro slip and localization in polycrystalline materials under uniaxial tension, Int. J. Plast. 108 (2018) 88–106.
- [98] J.M. Hestroffer, M.I. Latypov, J.C. Stinville, M.A. Charpagne, V. Valle, M. P. Miller, T.M. Pollock, I.J. Beyerlein, Development of grain-scale slip activity and lattice rotation fields in Inconel 718, Acta Mater. (2022), 117627.
- [99] V. Wan, M. Cuddihy, J. Jiang, D. MacLachlan, F. Dunne, An HR-EBSD and computational crystal plasticity investigation of microstructural stress distributions and fatigue hotspots in polycrystalline copper, Acta Mater. 115 (2016) 45–57.
- [100] M. Yaghoobi, Z. Chen, V. Sundararaghavan, S. Daly, J.E. Allison, Crystal plasticity finite element modeling of extension twinning in WE43 Mg alloys: calibration and validation, Integr. Mater. Manuf. Innov. 10 (3) (2021) 488–507.